SYNTHESIS OF NEW SOLID-STATE MATERIALS BY ULTRAHIGH PRESSURE TECHNIQUES

by

A. J. DeLai
R. M. Haag
T. Vasilos

Prepared by

AVCO MISSILES SPACE, AND ELECTRONICS GROUP
SPACE SYSTEMS DIVISION
201 Lowell Street
Wilmington, Massachusetts

AVSSD-0314-66-RR
Contract AF19(628)-2943
AFCRL-66-737

Project No. 5621
Task No. 562105

FINAL REPORT

Period Covered: 14 May 1963 thru 14 October 1966

20 December 1966

Prepared for

AIR FORCE CAMBRIDGE RESEARCH LABORATORIES
OFFICE OF AEROSPACE RESEARCH
UNITED STATES AIR FORCE
Bedford, Massachusetts 01730

AFCRL 66-737

This document consists of 122 pages,
201 copies, Series A

SYNTHESIS OF NEW SOLID-STATE MATERIALS BY ULTRAHIGH PRESSURE TECHNIQUES

by

A. J. DeLai
R. M. Haag
T. Vasilos

Prepared by

AVCO MISSILES SPACE, AND ELECTRONICS GROUP
SPACE SYSTEMS DIVISION
201 Lowell Street
Wilmington, Massachusetts

AVSSD-0314-66-RR
Contract AF19(628)-2943
AFCRL-66-737

Project No. 5621
Task No. 562105

FINAL REPORT

Period Covered: 14 May 1963 thru 14 October 1966

20 December 1966

Prepared for

AIR FORCE CAMBRIDGE RESEARCH LABORATORIES
OFFICE OF AEROSPACE RESEARCH
UNITED STATES AIR FORCE
Bedford, Massachusetts 01730

ABSTRACT

The microstructure and physical properties of dense oxides prepared at ultra-high pressure and low temperature have been studied. Completely dense, transparent magnesium oxide has been prepared in submicron grain sizes with hardness values twice that of single crystal material and 30 to 50 percent greater than that of hot pressed material. A new modification of samarium oxyhydroxide has been found and characterized. X-ray determinations of the compressibility of alkali halides (RbCl, RbBr) are reported.

Unclassified report

EDITED BY:
EDITORIAL SERVICES SECTION
R. L. TUCKER

CONTENTS

CONTENTS (Concl'd)

ILLUSTRATIONS

ILLUSTRATIONS (Cont'd)

ILLUSTRATIONS (Concl'd)

TABLES

ACKNOWLEDGMENT

It is a pleasure to acknowledge the assistance of Mr. J. Hill who performed the X-ray diffraction analyses and provided measurements of grain size, Dr. R. Duff and Mr. P. Burnett who made the electron microscopic examination, and Mr. R. Gardner of the Ceramographic Laboratory.

Messrs P. Foley, H. Surette and R. Martineau assisted in the setup and conduct of the experiments in the high pressure apparatus. Special note should be made of the contribution by the personnel of the Applied Mechanics Section, particularly Mr. R. Kelly who contributed the elastic analysis of the high pressure apparatus.

Finally our special thanks go to Dr. Johannes Plendl, and Mr. Lawrence Mansur of the Air Force Cambridge Research Laboratory for their support and encouragement of this work.

I. INTRODUCTION AND HISTORICAL SUMMARY

The advent of man-made diamonds has greatly stimulated interest in high pressure as a research tool. James Hannay, Henri Moissan, and others had investigated high pressures in the hope of making diamonds.[1] However, not until Professor P. Bridgman began his studies in the early 1900's was high pressure systematically studied.[2] He investigated the effects of high pressure on chemical reactions,[3] densities,[4] synthesis of new materials,[5] and compressibilities.[6,7] These classic studies, which culminated in the development of the "belt" apparatus[8] and the synthesis of diamonds,[9] have led to greatly expanded programs of high-pressure research both in this country and abroad.

It is not appropriate here to review all of these studies, but excellent reviews have been provided by K. L. DeVries, et al,[10] L. Berg,[11] and A. Zeitlen.[12] Continuing bibliographic coverage has been undertaken by H. T. Hall.[13]

It is worth noting that the studies have fallen into several broad categories. First, after the disclosure of the belt apparatus, the synthesis of new compounds and the formation of new, denser phases was extensively studied. Second, physical measurements at high pressure for clarifying the problems associated with solid-state physics and geology have been made. At present, this is the broadest field. Third, the application of high-pressure techniques to the fabrication of ceramics with improved properties resulting from the control of the microstructure has been actively studied at Avco.

The purpose of this work was the exploration of the realm of ultrahigh pressures and temperatures in synthesizing new solid-state materials, the study of pressure and temperature effects on possible phase transitions, the investigation of high pressure densification on such materials such as MgO, NiO, Cr_2O_3, Y_2O_3, lanthanide and actinide oxides, cubic BN, and possible combinations of these materials, and the study of the resulting structures and physical properties of newly obtained substances. In addition, measurements of the compressibility of metal halides, as well as sound velocities through various oxide materials, were made.

II. EXPERIMENTAL DEVELOPMENT OF APPARATUS

A. INTRODUCTION

To achieve the high pressures necessary for the effort, an apparatus had to be designed capable of providing pressures in the range of tens to hundreds of kilobars.

It is well known from elastic analysis that in a thick-walled cylinder subjected to hydrostatic pressure from the inside, the stresses are greater on the inner wall. However, it has been observed repeatedly that plastic flow on the inner wall results in a transference of the load to the outer wall which fails first. In order to overcome this tendency for the failure to originate at the outer wall, a series of concentric rings may be fitted together such that one ring is in compression and the other is in tension. The stress distribution throughout the rings can be arranged so that the proportional limit of the sustaining rings is not exceeded.

B. APPARATUS

1. Apparatus Design

In the design used, the die body proper was prepared from cobalt-bonded tungsten carbide, a composite which exhibits essentially no plastic flow. Similarly, the steel supporting rings used were unusually hard. With such materials it was possible to employ a classical elastic analysis[14] and treatment. In order to reduce the tensile stress at the interior wall of the die body, the die was put under initial compression by means of a series of surrounding steel rings. The interferences between these rings were so calculated that:

a. at the highest pressure of operation, the tensile stress on the inside wall of the die body did not exceed the proportional limit for such material,

b. in the unloaded condition, the compressive stress at the same place did not exceed the proportional limit,

c. conditions a. and b. were observed at each interface in the die proper after assembly, and

d. during assembly, the proportional limit was not exceeded in any subassembly.

2. Design Calculations

Two design approaches are appropriate. In the first case, the stresses at each interface may be preset and the interferences required to achieve these stresses may be calculated. In the other case, interferences may be estimated, the stresses calculated and the interferences adjusted as necessary in successive iterations. The 1×10^6 psi die body was calculated in this way on the basis of previous experience with similar designs. The stresses were acceptable on the first try and no iterations were necessary. A second apparatus was designed to provide a maximum working pressure of 3×10^6 psi (200 kilobar). In this case, the calculations after four iterations gave acceptable stresses which are shown below. Both the die body itself and the punches required this support and calculations were made for both.

The quantities calculated are contact pressure p (radial) and tensile and compressive stress f_t and f_c (circumferential) at each interface. These quantities are given by

$$p = \frac{E\,\delta}{b} \frac{(b^2 - a^2)\,(c^2 - b^2)}{2b^2\,(c^2 - a^2)} \tag{1}$$

$$f_t = \frac{b^2\,p}{c^2 - b^2} \left(1 + \frac{c^2}{2}\right) \tag{2}$$

$$f_c = \frac{b^2\,p}{b^2 - a^2} \left(1 + \frac{a^2}{2}\right) \tag{3}$$

where

- p = contact pressure at ring
- E = Young's Modulus
- δ = interference between rings
- c = outside radius of assembly
- b = outside radius of ring being pushed in
- a = inside radius of ring being pushed in
- f_t = tensile stress
- f_c = compressive stress

3. Assembly and Test

The geometry is shown in Figure 1. Typical calculations for the 1×10^6 psi cell are given in Appendix A. The results for a punch assembly are summarized in Table I for the 1×10^6 psi and Table II for the die assembly of the 3×10^6 psi apparatus which shows the stresses in the final assembly in both the loaded and unloaded condition.

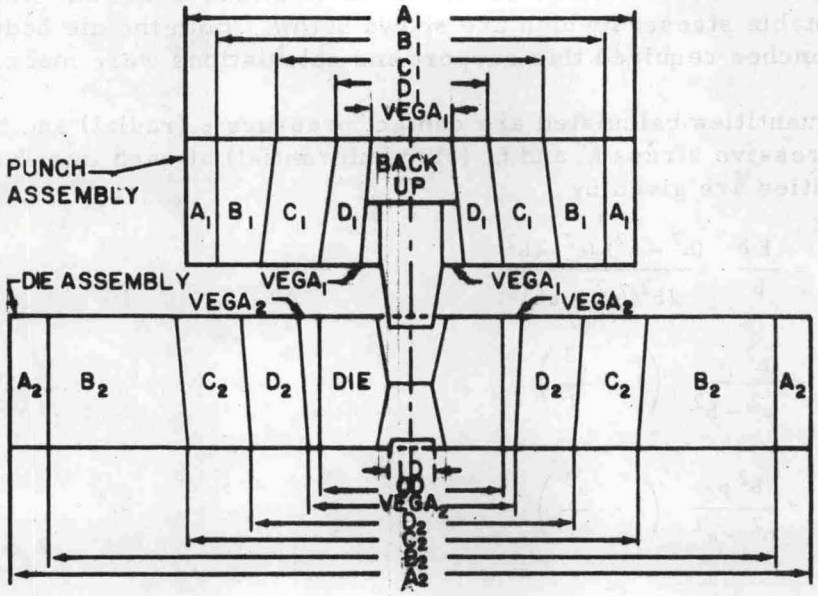

Figure 1 DIE OR PUNCH GEOMETRY

TABLE I

STRESS DISTRIBUTION FOR 1×10^6 psi PUNCH ASSEMBLY

Position	Rings ABC (psi)	Rings ABCD (psi)	Total Assembly Unloaded (psi)	Total Assembly Loaded (psi)
o.d. A	$f_t = 28,000$	$f_t = 67,600$	$f_t = 76,900$	$f_t = 98,700$
AB interface	$p = 23,000$	$p = 126,000$	$p = 254,000$	$p = 554,000$
o.d. B	$f_t = 33,050$	$f_t = 80,050$	$f_t = 91,050$	$f_t = 116,750$
i.d. B	$f_c = 57,000$	$f_t = 15,700$	$f_t = 141,250$	$f_t = 181,250$
BC interface	$p = 23,000$	$p = 126,000$	$p = 254,000$	$p = 554,000$
o.d. C	$f_t = 51,100$	$f_t = 124,200$	$f_t = 32,750$	$f_t = 73,000$
i.d. C	$f_c = 80,000$	$f_t = 15,700$	$f_t = 98,000$	$f_t = 178,000$
CD interface		$p = 103,000$	$p = 231,000$	$p = 531,000$
o.d. D		$f_c = 163,000$	$f_c = 128,000$	$f_c = 49,000$
i.d. D		$f_c = 264,000$	$f_c = 128,000$	$f_c = 164,000$
D Vega interface			$p = 128,000$	$p = 428,000$
o.d. Vega			$f_c = 128,000$	$f_c = 428,000$
Punch (center)			$f_c = 256,000$	$f_c = 821,000$

TABLE II

STRESS DISTRIBUTION FOR 1×10^6 psi DIE ASSEMBLY

Position	Rings ABC (psi)	Rings ABCD (psi)	Total Assembly Unloaded (psi)	Total Assembly Loaded (psi)
o.d. A	$f_t = 12,564$	$f_t = 33,060$	$f_t = 47,563$	$f_t = 50,063$
AB interface	$p = 11,458$	$p = 55,307$	$p = 144,037$	$p = 924,037$
o.d. B	$f_t = 13,714$	$f_t = 36,068$	$f_t = 51,886$	$f_t = 54,613$
i.d. B	$f_c = 37,780$	$f_t = 1,387$	$f_t = 29,103$	$f_t = 33,880$
BC interface	$p = 11,458$	$p = 55,307$	$p = 144,037$	$p = 924,037$
o.d. C	$f_t = 24,029$	$f_t = 63,196$	$f_t = 91,912$	$f_t = 96,689$
i.d. C	$f_c = 49,240$	$f_t = 15,096$	$f_t = 60,535$	$f_t = 68,385$
CD interface		$p = 43,849$	$p = 132,579$	$p = 912,579$
o.d. D		$f_c = 101,980$	$f_c = 56,541$	$f_c = 48,691$
i.d. D		$f_c = 145,830$	$f_c = 42,576$	$f_c = 24,776$
D-Vega interface			$p = 88,730$	$p = 868,730$
o.d. Vega			$f_c = 92,400$	$f_c = 74,600$
i.d. Vega			$f_c = 93,000$	$f_c = 70,050$
Vega-Die interface			$p = 88,730$	$p = 868,730$
i.d. Die			$f_c = 181,000$	$f_c = 599,000$

In order to compare the theoretical calculations with the actual stresses, strain gages were mounted on the outermost ring of the assembly. As each ring was assembled, the stresses were recorded and compared to the theoretical results. As indicated in the appendix, a 7.63-percent difference exists between the actual stresses and the calculated values on the average. These values are within specifications. On completion of the assembly of the apparatus, it was installed in the 400-ton press. Figure 2 shows the apparatus in place.

C. EXPERIMENTAL PROCEDURES

1. Pressure Calibration

The actual pressure in the apparatus had to be determined before any pressure runs could be made. The pressure calibration of the apparatus was accomplished by measuring the load required to convert Bi-I to Bi-II and Bi-II to BI-III. The bismuth wire in this instance was enclosed by previously melted and cast AgCl. The AgCl acted as a nearly hydrostatic pressure transmitting medium.

The mean transition pressure for Bi I→Bi II is 24, 410±95 bars (1 bar= 14.5 psi) and for Bi II→Bi III is 26,975±100 bars as determined by Kennedy and Lamori[15]. These transitions were determined by observing the discontinuity in resistance of the bismuth wire when it was placed in a sample of AgCl, as shown in Figure 3. A typical calibration curve is given in Figure 4 which shows a sharp change at the transition point when E/I is plotted versus load. At the point where Bi I→Bi II the pressure required is 25,410±95 bars.

2. Temperature Measurement

After the apparatus was calibrated for pressure versus load, it was necessary to measure the temperature of the sample versus electrical power input. This was accomplished by placing a thermocouple in the sample as shown in Figure 5. The couple was placed in the center of the sample and insulated from the resistance heater with Al_2O_3 tubes which extended out to the pyrophyllite gasket material. The couples were connected to a strip chart recorder.*

There were various types of thermocouples that could be used for these temperature measurements. H.M. Strong and R.E. Hanneman[16] have shown, however, that at low pressures one could use Pt-Pt+10 percent Rh couples without any large temperature correction.

---

*Leeds and Northrop type G, Speedomax.

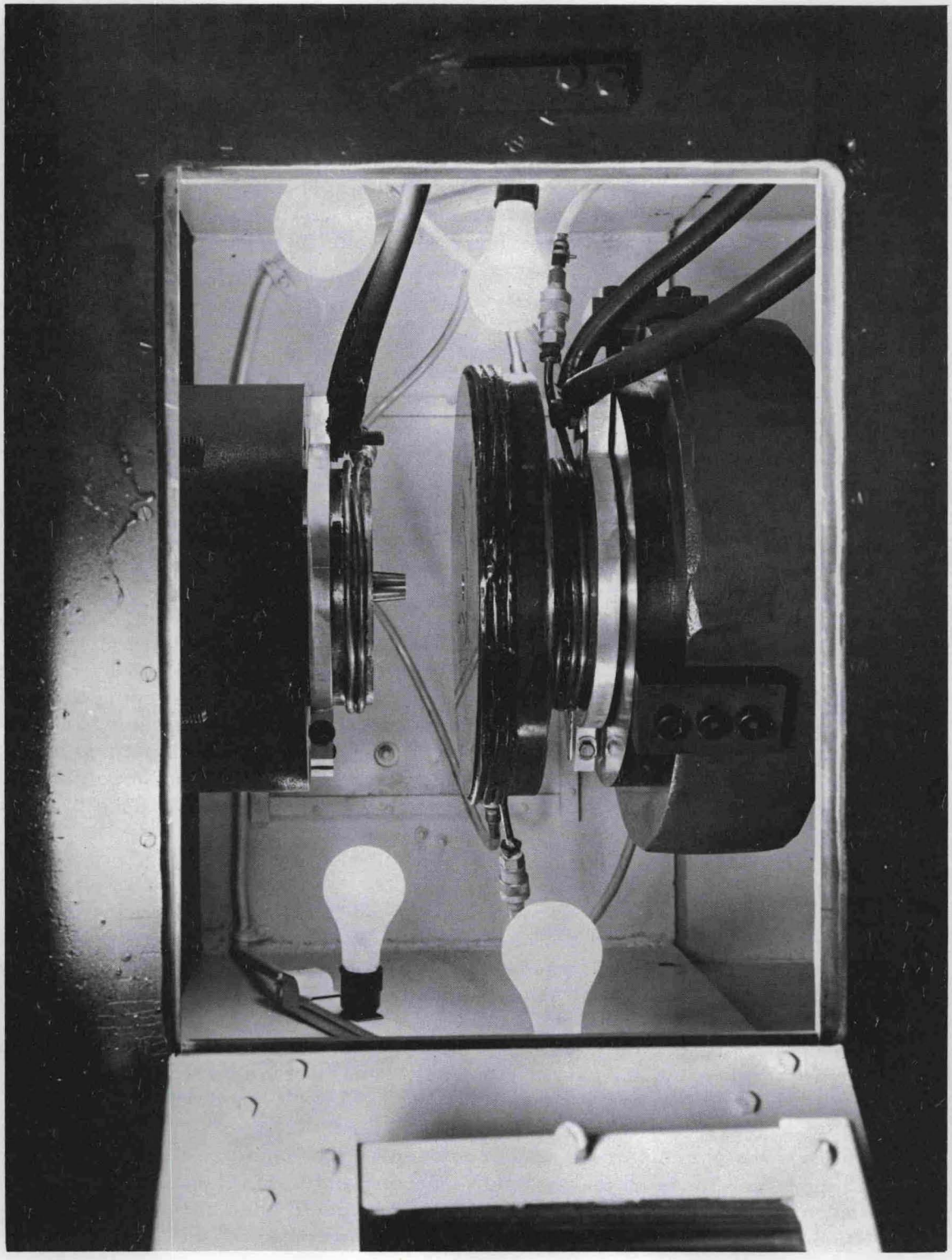

Figure 2 APPARATUS AND PLACE

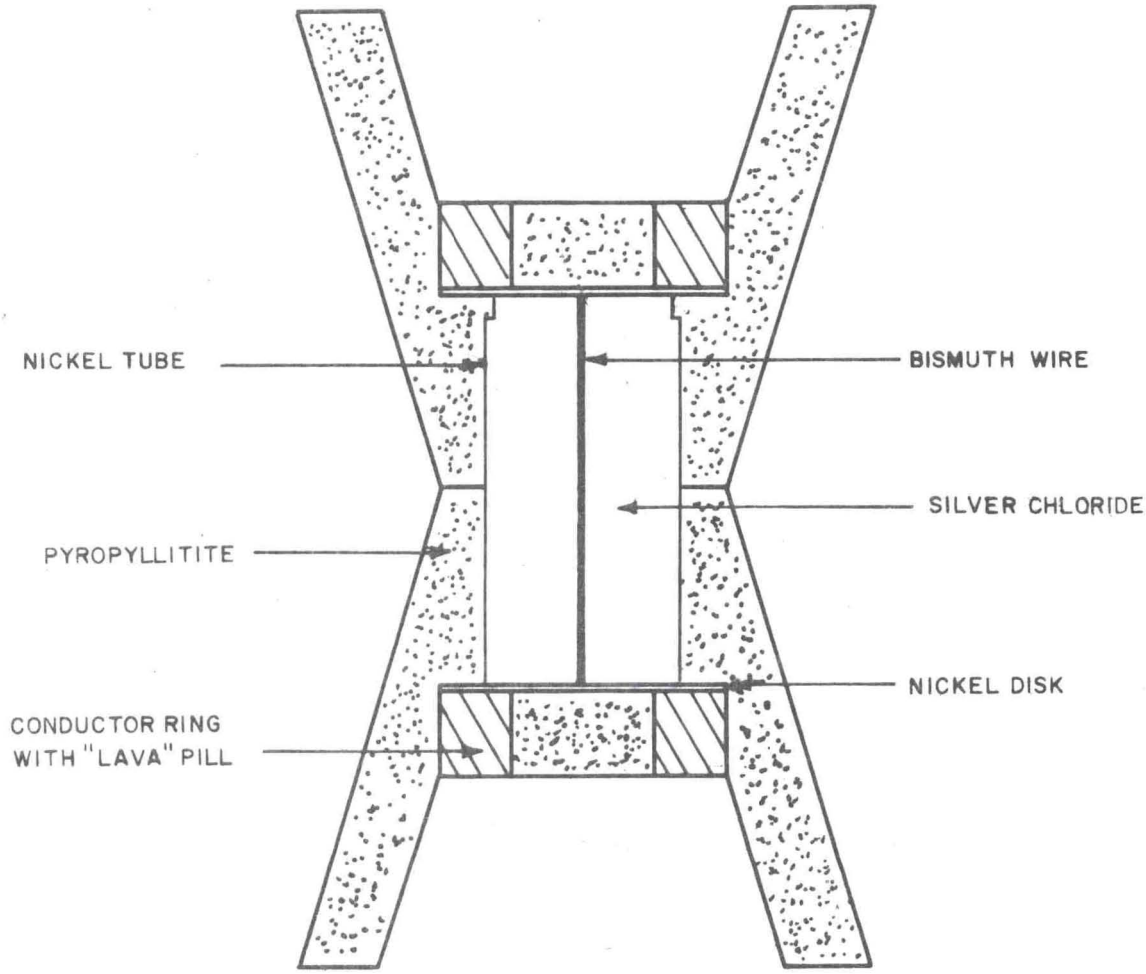

Figure 3 SAMPLE GEOMETRY FOR PRESSURE CALIBRATION

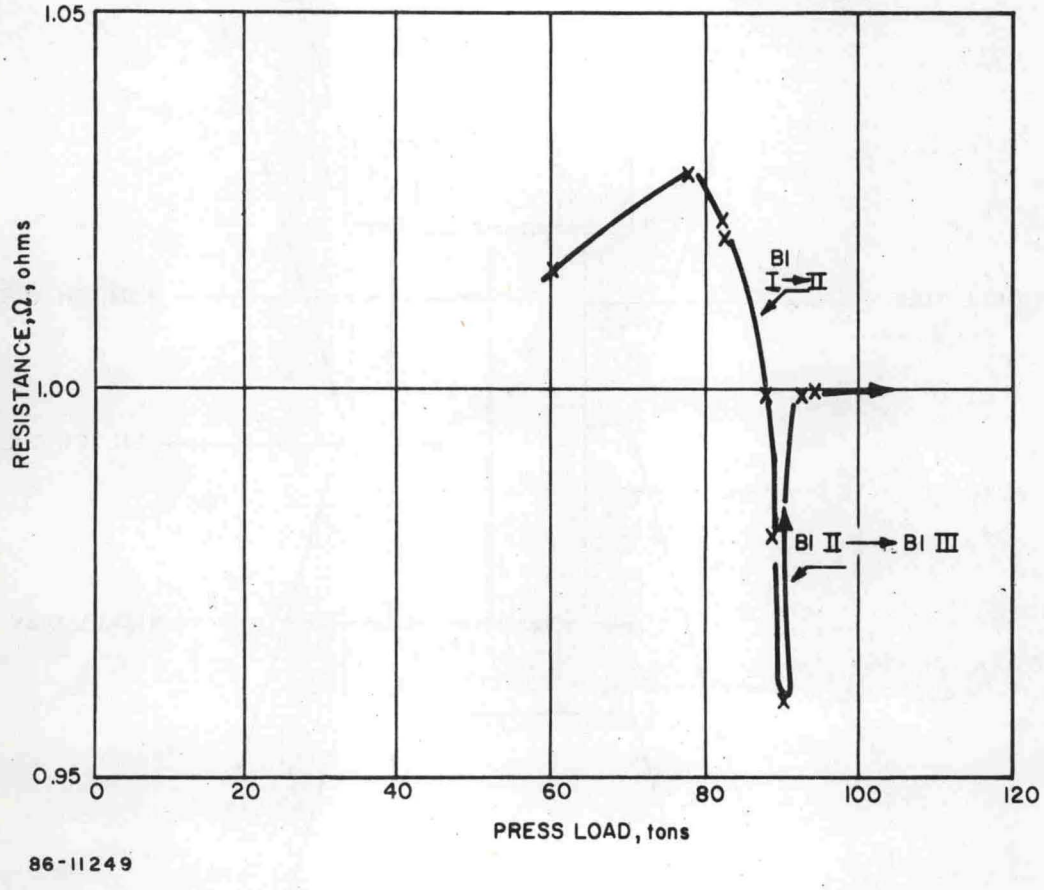

Figure 4 CALIBRATION (PRESSURE)

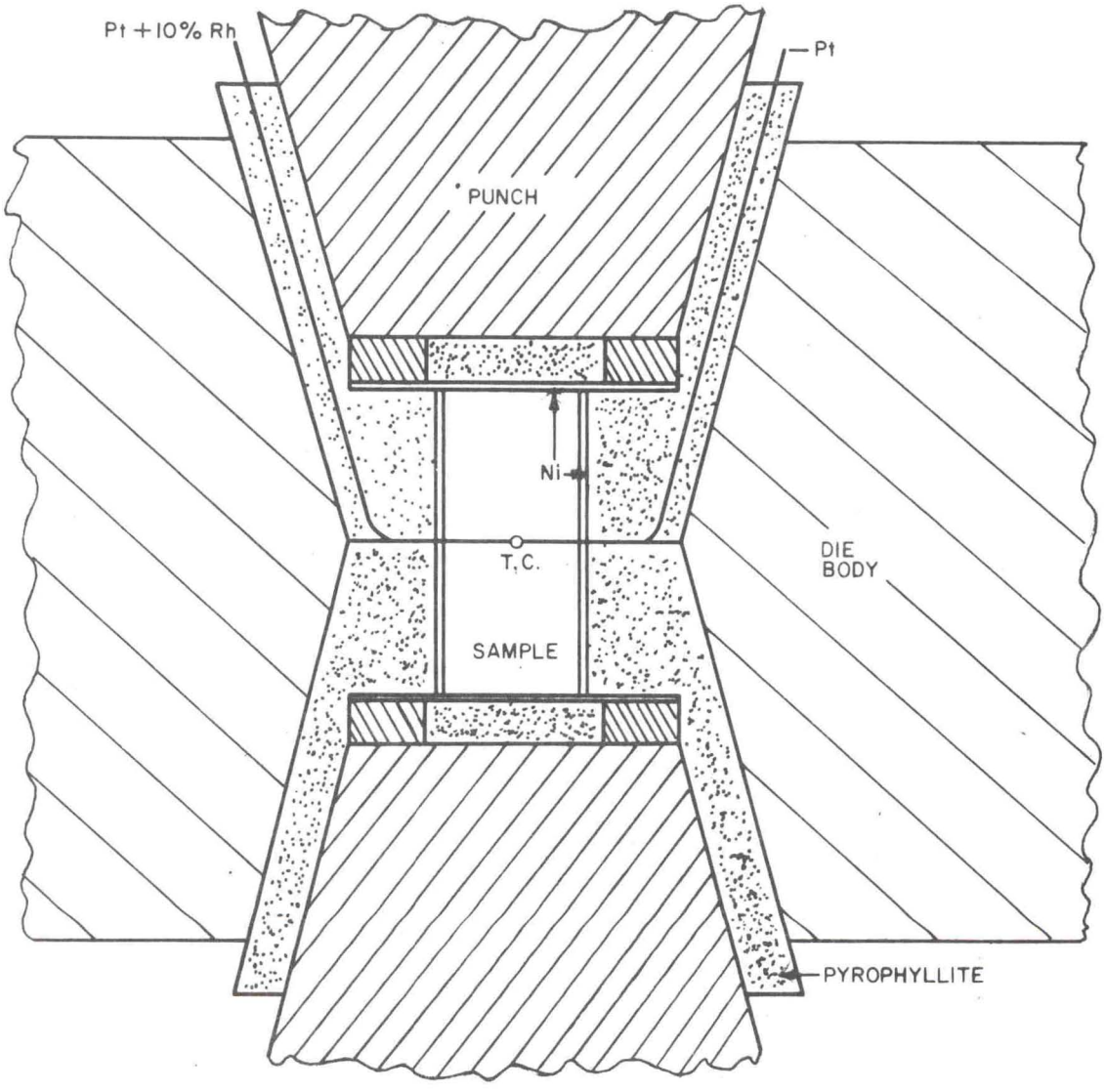

Figure 5 SAMPLE GEOMETRY FOR OXIDE DENSIFICATION STUDIES

The temperature observed was plotted against the power input. This curve gave a direct relationship of power versus temperature within 20° C, which was useful in the event the thermocouple opened during subsequent runs. In all cases where a thermocouple was used, a curve was obtained for the power input versus temperature.

3. Sample Design

The majority of experiments conducted in the 1 x 10^6 psi apparatus contained samples which were 0.500-inch in diameter by 1.000-inch long. The sample was placed inside of a tube which was either metal or graphite for resistance-heating purposes. The sample was enclosed by electrically conducting materials at each end of the sample. The remaining part of the sample was enclosed by pyrophyllite. The pyrophyllite, sometimes called "lava", is a fairly inert and stable material which acts as a pressure transmitting medium as well as an electrical insulator, and served as a gasket to maintain the sample under load. A schematic diagram of the sample is shown in Figure 5.

D. TECHNIQUES--TYPICAL RUN

A typical run containing MgO, NiO or Cr_2O_3 was set up as follows. The oxide was preheated to at least 600° C for 8 hours to drive off any volatiles that might be present. The powder was then placed into a polyvinyl chloride bag and pressed isostatically to 22,000 psi. The piece was removed, crushed, and prepressed at 35,000 psi. After removal from the isostatic press, it was then machined to fit the resistance heater. The sample was placed into the pyrophyllite gasket and loaded into the die body. With the previously aligned punches in place in the 400-ton press, the die was put in place on the lower punch. Thermocouple and strain gage loads were attached as required. Although the specific program varied with the sample and experiment, typically the sample was brought to the desired pressure by adjusting the press load to that indicated by the calibration runs. The temperature was then raised to the desired value by resistance heating of the metal or graphite sleeve. The attainment of the desired temperature was judged either by direct indication from internal thermocouples or by matching power-temperature curves with previous runs. In those runs, where new phases, possibly only metastable at lower temperature and pressure were sought, the sample was "quenched" by simultaneous removal of pressure and electrical power. In other cases where dense ceramic pieces were desired, a programed reduction of both pressure and temperature was followed to minimize mechanical and thermal shock.

Upon completion of the run, the sample along with the metal or graphite heater, was removed from the apparatus. The resistance heater was removed and the sample was exposed. The sample was examined by electron microscopy, X-ray diffraction or metallography.

III. EXPERIMENTAL INVESTIGATIONS

A. TRANSFORMATION OF PREVIOUSLY KNOWN HIGH-PRESSURE PHASES

1. Cubic BN

Another new material which has been synthesized since the advent of man-made diamonds is the cubic form of boron nitride.

Boron nitride, isoelectronic with carbon, is known to exist in two modifications.[17] The hexagonal modification which has many properties similar to those of graphite is well known. A metastable modification is cubic and has the sphalerite structure of the diamond and many of the properties of the diamond including high hardness. At high pressure and temperature, this modification becomes stable relative to the hexagonal modification. The transformation is slow, however, except in the presence of some catalyst. The best catalyst appears to be Li_3N.

Lithium nitride was prepared by reacting metallic lithium with ammonia gas or dry nitrogen according to the following schemes:

$$3\ Li + NH_3 \rightarrow Li_3N + 1\text{-}1/2\ H_2$$

or

$$3\ Li + 1/2N_2 \rightarrow Li_3N$$

Both of these reactions go readily at moderate temperature, and both reactions were used to prepare catalyst for these runs. It was observed, however, that the material prepared by the second reaction was more stable in air atmosphere and did not appear to react as rapidly with the moisture in the air. Only this second material was used for the synthesis runs.

Samples were prepared by packing a layer of powdered hexagonal boron nitride in a graphite heater tube (rather than nickel which is attacked by the lithium nitride) sprinkling in crushed lithium nitride, adding another layer of boron nitride, packing and adding catalyst and repeating about five times. Molybdenum end discs closed the system. The sample was placed in the die with the usual pyrophyllite insulator.

Since these samples were not prepressed, the packed density was relatively low. This gave a large compression ratio at synthesis pressures which would have resulted in thermocouple failure, and thermocouples were therefore not installed. The temperature of reaction was not measured, but was estimated from the power input.

Five runs are summarized in Table III. After run No. 3, at an estimated pressure of 7×10^5 psi, examination of the sample revealed amber colored crystals which resembled boron cubic nitride. These crystals were too small to isolate for X-ray diffraction.

TABLE III

CUBIC BORON NITRIDE PREPARATIONS

Run No.	Pressure (psi)	Power (watts)	Results
1	7×10^5	No heat	Die cracked
2	7×10^5	1028	Too low temperature
3	7×10^5	1428	Amber colored crystals formed
4	7×10^5	1506	No change in hex BN
5	7×10^5	No heat	Die cracked

2. Coesite

a. Introduction

Although silicon is one of the most abundant elements of the earth and quartz or silicon dioxide is one of the most common rock-forming minerals, not until 1953 did anyone realize that a high-pressure modification of silica existed.

In 1953 a dense polymorph was synthesized by Dr. L. Coes, Jr.[18] of Norton Co. This new dense form was named Coesite or silica C. This material was made at pressures of about 35 kilobars in the temperature range of 500° to 800° C. This same material was later found in nature at Meteor Crater, Arizona.

Another dense form of SiO_2 was synthesized by Stishov and Popova[19] (1961) at 1200° to 1400° C at pressures above 160 kilobars. The material has been found in the Coesite bearing Coconino Sandstone[20] of Meteor Crater, Arizona. This dense form made at very high pressures was named Stishovite in honor of the discoverers.

b. Experimental Investigation

Fused silica was pressed at a pressure of 35 kilobars at a maximum temperature of 640° C for 5 to 10 minutes. Preliminary examination by the Becke method of determining refractive indices revealed the possible presence of Coesite which is a denser form of SiO_2. To confirm this result, a Debye-Scherrer X-ray pattern was obtained for analysis.

Natural α-quartz was crushed and subjected to high pressure of 40 kilobars and temperature of 550° C for 20 to 65 minutes. Debye-Scherrer X-ray powder patterns were again taken of this pressed material. The "d" values obtained indicated the presence of α-quartz with two strong lines (d values of 3.10 and 3.45), corresponding to the strongest lines of Coesite. The amount of Coesite present was very small. The Coesite was formed in these experiments at the minimum pressure and temperature necessary for direct conversion of the low-density silica to the high-density silica.

B. HALIDES

NaI powder obtained from Fisher Chemicals was melted and cast into a nickel tube. After placing the sample into the high-pressure apparatus, the NaI was subjected to a pressure of 25×10^4 psi and a constant power input of 550 watts. The sample had compressed 36 percent of its original volume. The volume change caused the thermocouple to open.

These initial experiments indicated no metastable phase present as determined by X-ray diffraction.

C. RARE EARTHS

The rare earths, that is the sesquioxides, are found in three distinct structural forms. The first of these is the hexagonal or A-R_2O_3 structure which is typified by La_2O_3. The second is the monoclinic or B-R_2O_3 structure and the third is the cubic or C-R_2O_3 structure which is the same as that of Mn_2O_3. In general, the rare earth metal ions with the largest radii; e.g., lanthanum, form the hexagonal oxide, and those with the smallest radii form the cubic oxide. Many of the rare earths can be obtained in two modifications. Thus, samarium oxide is found in both the cubic-C and monoclinic-B forms.

Investigations of the stability limits of the various structural modifications have been carried out for a number of years. The range of stability of the three modifications as a function of cation-radius and temperature as proposed by Shafer and Roy is shown in Figure 6. It is evident from this figure that samarium oxide lies near the border between the A- and B- type fields at high temperatures. However, the A-type oxide of samarium has not been observed either in high-temperature X-ray studies nor in room-temperature examination of material quenched from high-temperatures.

In the hexagonal oxide each cation has seven nearest oxygen neighbors compared with six such neighbors in the other structures. This results in a greater density in the hexagonal modification compared with the other two forms. Thus, in the case of neodymium oxide, the relative volumes are A:B:C = 75.5:77.7:84.6 (A^3/FW). It seemed that if the A-modification of Sm_2O_3 could be formed that both high-temperature and high pressure would be required. Accordingly, the material quenched from high temperatures at pressures to 30 kilobars was examined. In no case was any trace of an hexagonal modification observed.

Experimentally, C-form (cubic) oxide (a_o = 10.89A) obtained from Research Chemicals Corporation was prepressed in a steel die to approximately 50 percent of theoretical density. This compact was loaded into a nickel tube and into the high-pressure apparatus described previously. Some samples were instrumented with thermocouples, others were not. In the absence of such instrumentation the temperature of the run was estimated from the power settings as calibrated in the instrumented runs.

In eight runs (shown in Table IV) at 30 kilobars and temperatures between 575° and 925° C the C-form was converted to the more dense B-form. At the lowest temperature the conversion was incomplete. In two runs, one at 580° C and one at 925° C the monoclinic form was used as the starting material. No conversion of this oxide was observed.

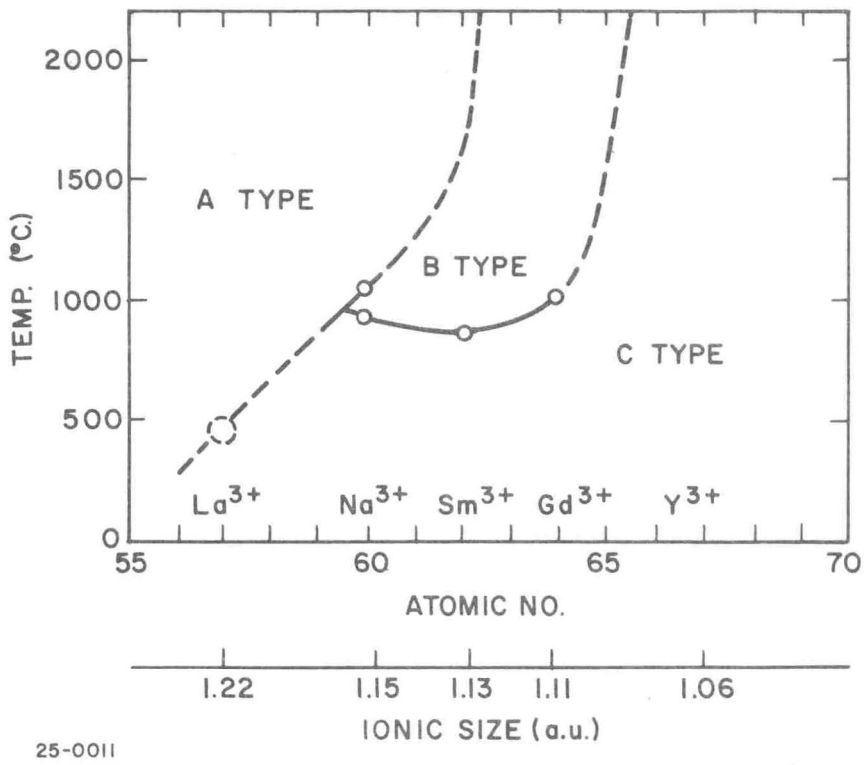

Figure 6 POLYMORPHISM OF RARE EARTHS AS A FUNCTION OF ATOMIC NUMBER

TABLE IV

SM_2O_3 RUNS

Run No.	Pressure (psi)	Temp. (°C)	Time (min)	Starting Oxide Material	Results
51	450,000	630	15	C-form	No analysis
52	450,000	575	15	C-form	B-form + C-form + "old" SmOOH
55	450,000	840	10	C-form	B-form + little "new" SmOOH
59	450,000	910	15	C-form	B-form + little "new" SmOOH
64	450,000	900	15	C-form	B-form + "new" SmOOH
65	450,000	875*	15	C-form	B-form + "old" SmOOH
66	450,000	780	15	C-form	Little B-form, mostly "new" SmOOH
67	450,000	700	10	C-form	B-form + "new" SmOOH
72	450,000	925	10	B-form	B-form + "old" SmOOH + "new" SmOOH + $Sm(OH)_3$ B-form
73	450,000	715	30	B-form	Runs made to determine optimum conditions of formation of β-SmOOH
92	450,000	550	1	C-form	
93	450,000	475	15	C-form	
95	450,000	510*	2	C-form	
96	450,000	920	1	C-form	
97	450,000	900	6	C-form	
99	450,000	930	17	C-form	
101	500,000	770	2	C-form	
103	500,000	690	13	C-form	Runs made to prepare single phase β SmOOH and search for single crystals. Product used. X-ray diffraction confirms new phase present in IR and X-ray studies. No single crystals isolated. X-ray diffraction confirms β-SmOOH present.
104	460,000	690	15	C-form	
107	500,000	650*	30	C-form	
161	500,000	630*	60	C-form	
162	500,000	665*	92	C-form	
163	480,000	670*	61	C-form	
164	480,000	670*	60	C-form	

*Temperature determined from power versus temperature curve.

X-ray diffraction analysis of the products of the high-pressure runs revealed, in addition to the two oxides, various hydroxides and oxyhydroxides. The water for the formation of these compounds comes from the decomposition at elevated temperature of the pyrophyllite gasket material. We have observed both of the previously reported hydroxides and the previously reported oxyhydroxide SmOOH. In addition, we have found a new phase which we call β-SmOOH.

Weight loss versus temperature curves from preparations showing only the X-ray diffraction lines of the new phase were obtained. These are shown in Figure 7. In each case the sample was heated in air for 1 hour at the indicated temperature, cooled, weighed and reheated to the next higher temperature. The weight loss begins above 300° C and constant weight is observed above 700° C.

In one case a small aliquot was taken for X-ray diffraction analysis after heating to 500° C. The curve shows this as a weight loss. The curve has not been renormalized for this loss since the displacement of the curve is small. Shown in the same figure is the expected weight loss assuming the starting material to be Sm_2O_3-H_2O. In a separate experiment a SmOOH was heated in vaccum to 700° C. The evolved gases were condensible at the temperature of liquid nitrogen and the weight loss was comparable to that reported above. Therefore, it is assumed that the new phase has the composition SmOOH.

Infrared measurements were made with a Perkin Elmer Model 221 spectrometer. The sample was scanned in the wavelength range from 2.5 to 16 microns using both KBr pellet and petrolatum mull techniques. The OH stretching vibration at 2.93 microns was observed together with the bending vibration at 6.8 microns. In addition, unassigned absorption peaks between 11 and 15 microns were observed.

Beta-SmOOH is light yellow in color. Since no single crystals could be isolated, optical properties could not be determined. It was, however, determined to be optically anisotropic with an average index of refraction of approximately 1.93.

The X-ray diffraction results are shown in Table V. These have been indexed on a tetragonal unit cell with $a_o = 8.102$, $c_o = 11.212$. The observed density, 6.62 grams per cc, gives 15.9 formula weights per unit cell. This is reasonable for a tetragonal structure. A structure with 16 formula units per unit cell and a theoretical density of 6.66 can therefore be assumed. As indicated above, no single crystals could be isolated and no more detailed studies could be performed.

However, it should be noted that by a 45-degree rotation around the C-axis, a nearly cubic cell can be obtained with sides averaging about 11.3 A which contains 32 formula units, that is $H_{32}Sm_{32}O_{64}$. This cube is only slightly larger than that of the defect fluorite lattice of cubic Sm_2O_3 and contains just enough excess oxygen ions to fill the vacancies in that structure. In fact, a fair fit of the stronger lines to a cube with $a_o = 5.70$ expedited the determination of the

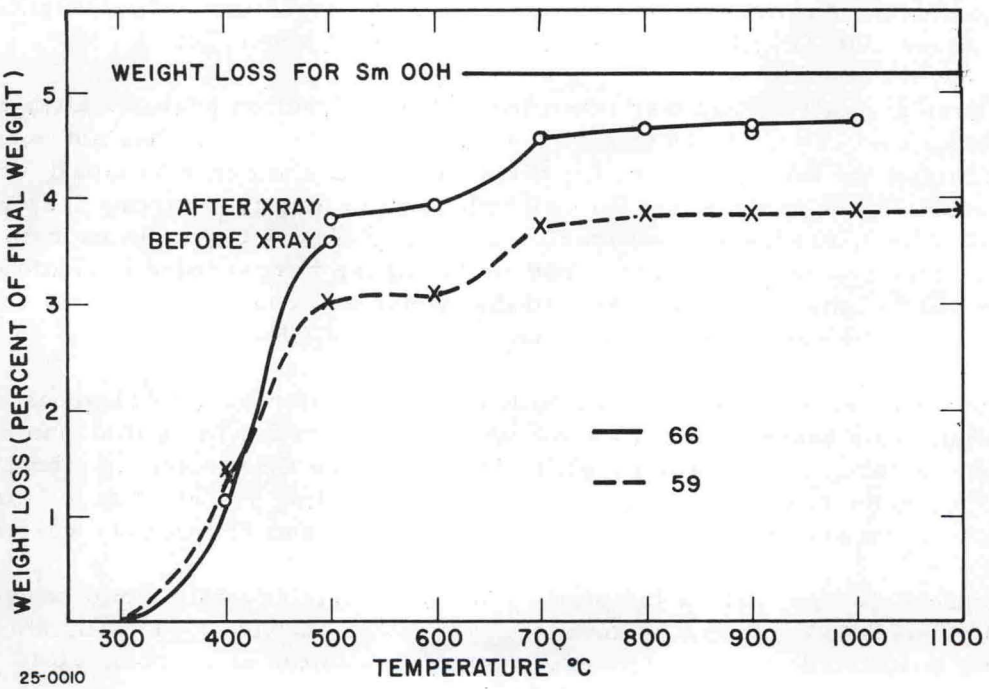

Figure 7 WEIGHT LOSS VERSUS TEMPERATURE FOR SmOOH

TABLE V

X-ray DIFFRACTION RESULTS βSmOOH

hkl	d_{obs}	d_{calc}	$d_{calc}-d_{obs}$	I/I_o
002	5.609	5.606	-0.003	10
111	5.068	5.101	+0.033	3
112	4.004	4.007	+0.003	9
202	3.290	3.283	-0.007	100
220	2.867	2.864	-0.003	50
004	2.814	2.803	-0.011	15
310	2.557	2.562	+0.005	10
222		2.551	-0.006	
204	2.309	2.305	-0.004	25
400	2.023	2.025	+0.002	22
224	2.002	2.003	+0.001	30
401		1.993	-0.009	
314	1.892	1.891	-0.001	9
331		1.882	-0.010	
332	1.804	1.808	+0.004	12
420		1.812	+0.000	
305	1.722	1.725	+0.003	28
422		1.724	+0.002	
206	1.698	1.697	-0.001	12
333		1.700	+0.002	
404	1.639	1.642	+0.003	7
423		1.630	-0.009	
502	1.563	1.559	-0.004	12
226		1.565	+0.002	
424	1.519	1.521	+0.002	10

tetragonal unit cell given above. It is reasonable then to postulate a structure based on the fluorite structure and to ascribe the shortening of the C-axis, relative to the A-axis to hydrogen bonding.

Beta-SmOOH is easily converted to the hydroxide by boiling in water for 15 minutes. After air drying at 110° C, the weight loss on ignition to 1100° C is 12.6 percent, corresponding to the loss of 1.49 moles of H_2O per mole of starting SmOOH. X-ray diffraction examination of this hydroxide gave the results shown in Table VI. These d-values have not been indexed and do not correspond to either of the two reported hydroxides as shown in the same table. Note that this hydroxide is not the same as the high pressure modification prepared by Shafer and Roy.

D. DENSIFICATION OF OXIDE CERAMICS

1. Introduction

The importance of microstructure (average grain size, grain size distribution, pore distribution, orientation, etc.) upon physical properties has become increasingly apparent. Typically, high density is achieved in ceramic materials sintering at high temperature. However, the employment of high temperature often leads to excessive grain growth with a subsequent deterioration in mechanical properties. Control of the densification process by void elimination mechanism and/or by small amounts of second phase additions have in some instances allowed the achievement of high density with small grain size. These techniques, however, are quite specific and applicable to a limited number of materials. In preliminary studies at Avco/SSD, fully dense magnesium oxide was produced by high-pressure techniques at relatively low temperatures resulting in an extremely fine grain size and high hardness number. In further effort, a program concerned with the densification processes was undertaken. For this study, two classes of materials were chosen, e.g., 1) nearly isotropic face centered cubic (rock-salt structure) oxides MgO and NiO and 2) anisotropic hexagonal oxides, Al_2O_3 and Cr_2O_3.

2. Experimental

a. Starting Materials

1) MgO -- except as otherwise noted, all the MgO employed was Fisher electronics grade with an average particle size of 300A as determined by X-ray diffraction line broadening or 500A as determined by electron microscopy. Before use, the material was preheated to 600° C in air atmosphere to decompose any brucite present and drive off any volatiles.

TABLE VI

COMPARISON OF X-ray RESULTS $Sm(OH)_3$

$Sm(OH)_3$ This Work		$Sm(OH)_3$ Hexagonal			$Sm(OH)_3$ High-Pressure Form	
d	I/I	d	I/I	hkl	d	I/I
5.609	80	5.54	100	(100)	7.816	25
3.296	5	3.16	70	(110)	5.566	35
3.251	60	3.03	55	(101)	3.723	80
3.084	100	2.734	15	(200)	3.363	5
2.780	20	2.183	90	(201)	3.089	40
2.423	8	2.064	15	(210)	2.852	5
2.222	70	1.821	50	(300)	2.768	25
2.099	15	1.795	65	(211)	2.583	100
1.848	35	1.575	15	(220)	2.089	30
1.824	55	1.519	7	(310)	2.057	5
1.751	8	1.400	20	(311)	1.843	45
1.599	25	1.366	10	(400)	1.819	5
1.537	6	1.284	10	(401)	1.596	15
1.415	13	1.194	10	(410)	1.592	10
1.384	6				1.548	20
1.307	8				1.534	10
					1.382	5
					1.290	10
					1.206	10
					1.204	5

2. Experimental

a. Starting Materials

1) MgO -- Except as otherwise noted, all the MgO employed was Fisher electronics grade with an average particle size of 300A as determined by X-ray diffraction line broadening or 500A as determined by electron microscopy. Before use, the material was preheated to 600° C in air atmosphere to decompose any brucite present and drive off any volatiles.

2) NiO -- Nickel oxide was prepared by the calcination at 1000° C for 24 hours of $NiSO_4 \cdot 6H_2O$ obtained from Allied Chemical. After calcination the average particle size was 2000 A as determined by electron microscopy examination

3) Cr_2O_3 -- Chromium oxide was prepared by calcination at 1000° C of chromium ammonium sulfate. After calcination, the average particle size was 3800A as determined by electron microscopy examination.

4) Al_2O_3 -- The aluminum used was Linde B, a mixture of γ alumina, with a grain size of 0.02 micron, and α-alumina with a grain size of 0.20 micron. These grain sizes were determined by electron microscopy.

b. Sample Preparation

The 1×10^6 psi apparatus with a 0.750-inch internal diameter provides for a sample diameter of 0.500 inch and a length of approximately 1 inch.

The starting material was formed into cylinders and isostatically prepressed to approximately 50 percent of theoretical density. After this prepressing, the sample was machined to the size indicated above, inserted into the heater casing and assembled with the pyrophyllite gaskets in the apparatus. When thermocouples were to be used, they were installed as described previously.

3. Results

a. MgO

The fabrication runs made in this program are summarized in Appendix C. Samples from runs 20 and 21 for example, were submitted to metallographic and electron microscopy determination of hardness, grain size and density. Both had been pressed at 250,000 psi at

approximately 1000° C. Sample 21A did not show any grains which could be measured. "Pores", however, were observed with an average size of approximately 500A, that is, of the same order as the starting powder. The shape of the "pores" suggested to the microscopist that they were pull-outs rather than real pores. Sample 20 showed better definition of the grains with some being extracted with the replica. The hardness measurements were 1187 and 1095 KHN (average of 5 each) with a 100 gram load. Electron micrographs of these two specimens are shown in Figure 8 and 9. A thin chip of sample 21 was chemically thinned for transmission electron microscopy. This is shown in Figures 10a & b at 240, 000X showing an average grain size of approximately 500A.

The early experiments with MgO, runs 10B and 12B had shown that essentially complete densification would be achieved with a minimum of grain growth and the development of high hardness. A study of the processing variables was made in runs 45C and 53C to 77C. The relation between temperature and time under pressure as independent variables and grain size and hardness as dependent variables was investigated. In this series, the pressure was kept constant at 110, 000 psi (7.5 kilobars). In Figure 11, the grain size as determined by X-ray line broadening is plotted against the temperature of the run. Above about 900° C considerable grain growth is evident although run 74C shows no appreciable grain growth, even at 1025° C. There is very little effect of time; most of the grain growth appears to develop within the first 10 minutes at temperature.

The results of Knoop hardness measurements are shown in Figure 12. Although the results are not conclusive, there is a definite evidence of a maximum at about 900° C. Above this temperature grain growth occurs, below this temperature insufficient densification is obtained. In Figure 13 the hardness is plotted against the grain size. The considerable scatter at small grain size reflects the differing degrees of densification in the various samples. Thus, the high values represent those specimens which had density without appreciable grain growth while the low values represent those specimens run at lower temperature which had not densified as much.

The extremely high hardness observed in these preparations suggested possible connections between hardness and optical properties, as suggested by the contract monitor. To evaluate this, a number of runs were made to prepare specimens exhibiting the high hardness observed in these experiments and these specimens were submitted to AFCRL for further study. They are listed in Table VII.

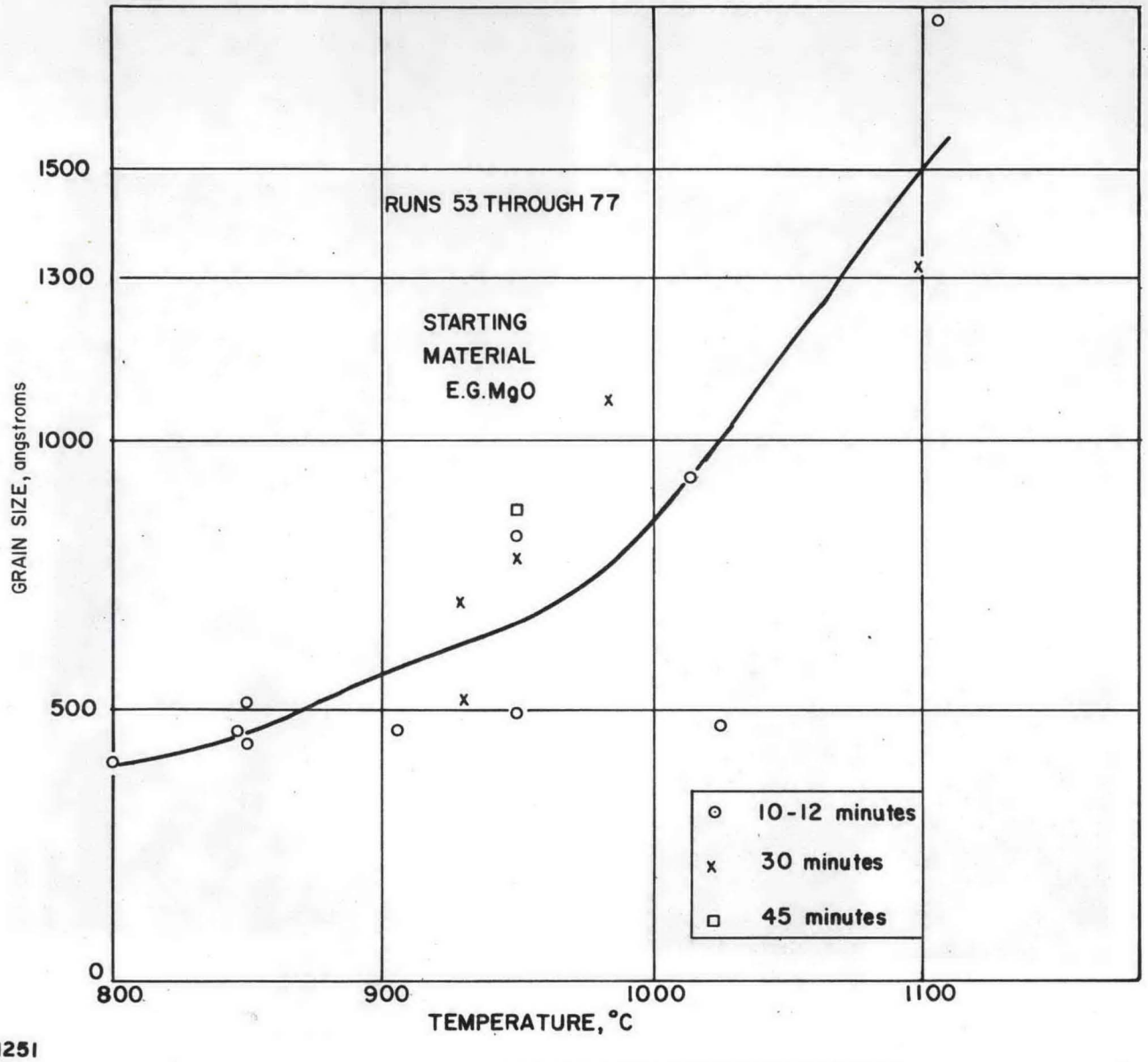

86-11251

Figure 11 GRAIN SIZE VERSUS TEMPERATURE

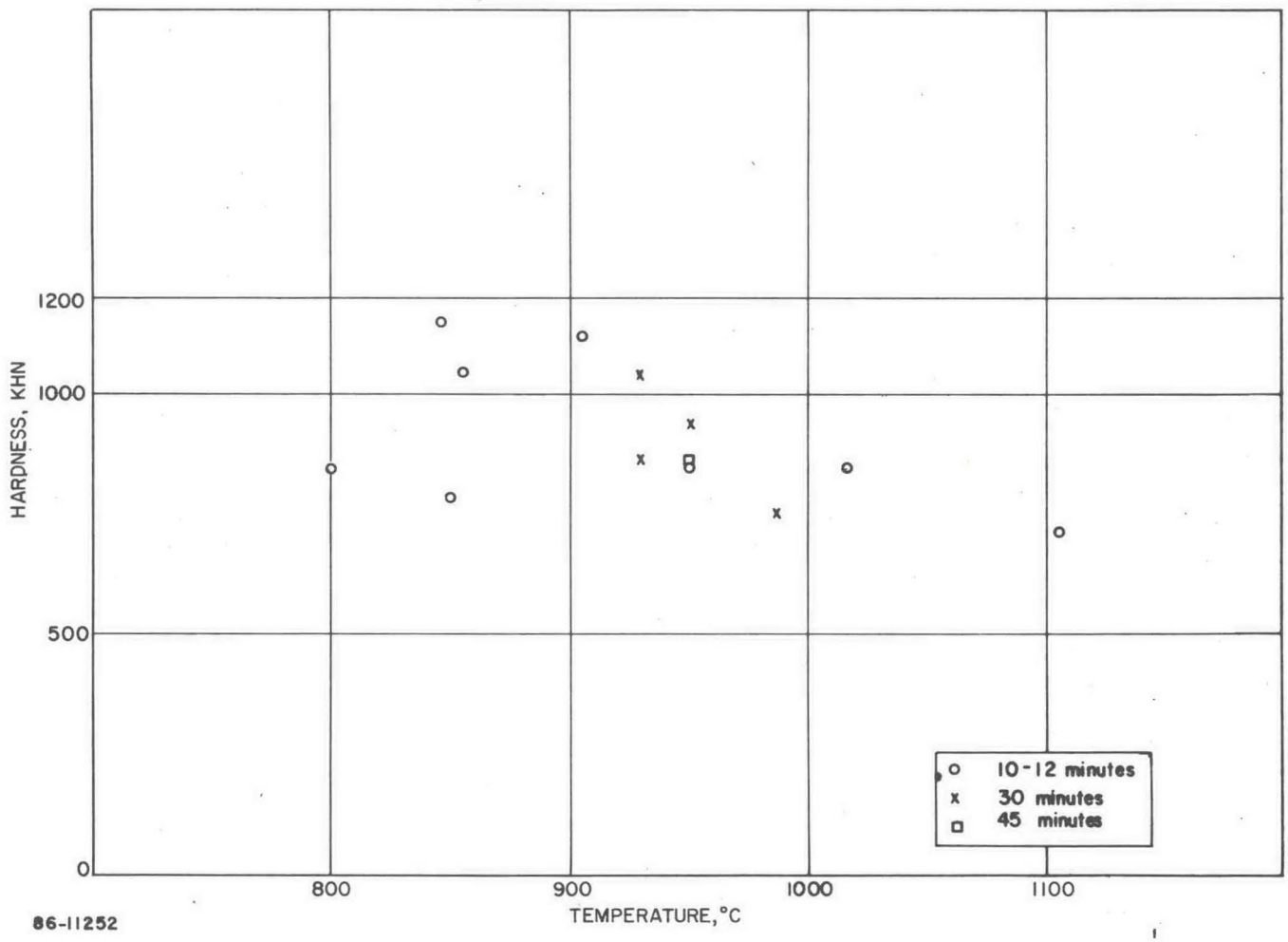

Figure 12 KNOOP HARDNESS VERSUS TEMPERATURE

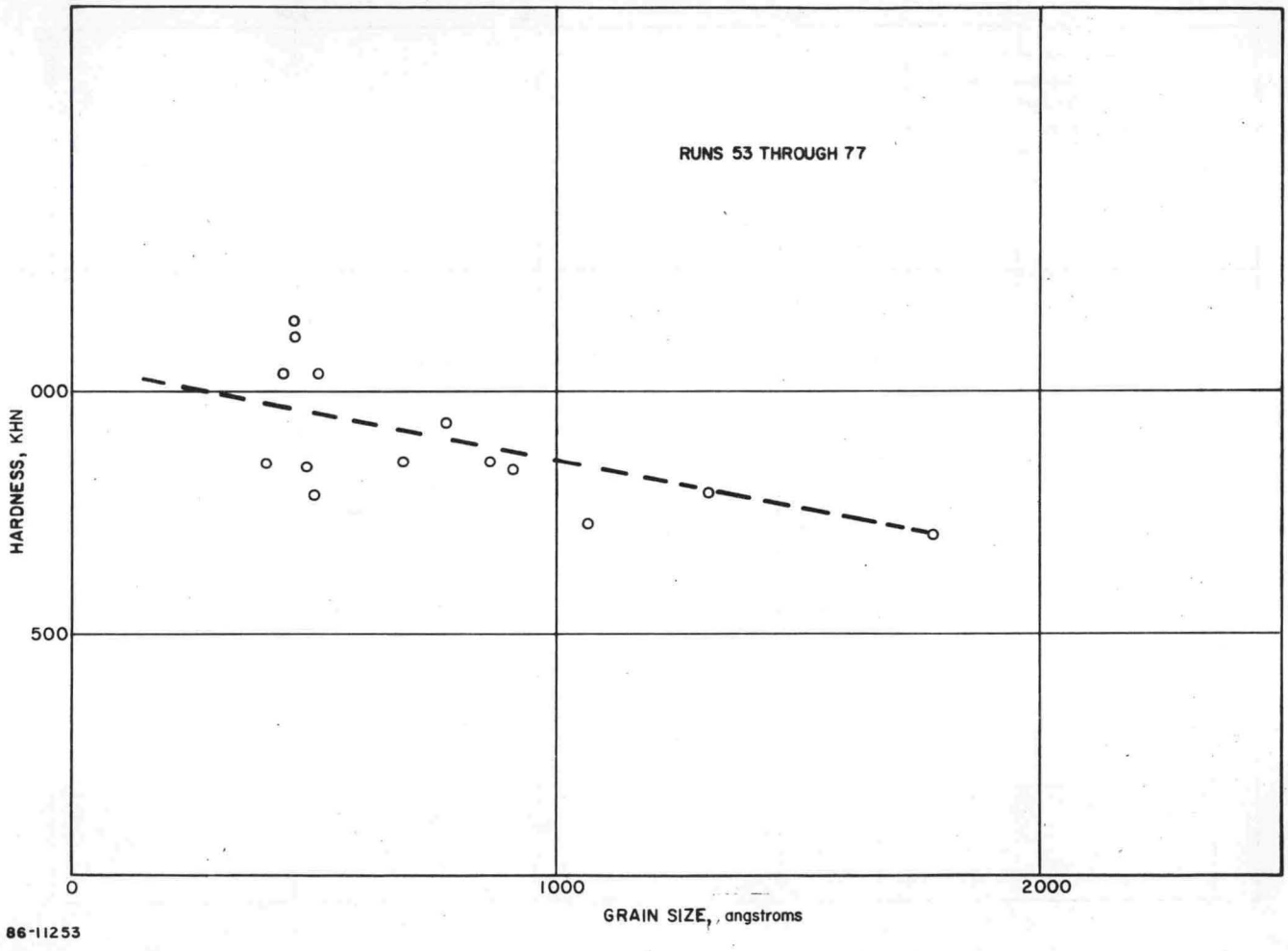

Figure 13 KNOOP HARDNESS VERSUS GRAIN SIZE

TABLE VII

MgO SAMPLES SENT TO AFCRL

Sample No.	Pressure (psi)	Temperature (°C)	Heater	Knoop Hardness
82	110, 000	800	Ni tube	759
83	110, 000	800	Ni tube	825
87	110, 000	990	Ni tube	--
88	110, 000	1105	Ni tube	--
735	6, 000	1150	Graphite die	636
2	6, 000	1300 to 1400	Graphite die	--
45	250, 000	~845	Ni tube	--

Some of the MgO specimens which were densified at temperatures below 800° C were dark blue, almost black. X-ray diffraction indicated that the blue specimens were mostly brucite ($Mg(OH)_2$) with minimum amounts of the starting material MgO. It is possible that the decomposition of the pyrophyllite gasket material yields considerable amounts of water vapor which could cause the observed hydration. Samples were examined by infrared spectroscopy* in the range 2.5 to 16 microns and showed strong evidence of (OH) in both the stretching and bending ranges.

By raising the temperature to 850° C this reaction was prevented and completely transparent pieces were obtained. One such piece is shown in Figure 14. Infrared analysis showed no evidence of (OH).

b. NiO

Nickel oxide preparations are listed in Table VIII. The most interesting sample was sample 32 which contained many single crystals of NiO. Some of these crystals were isolated and transmitted light photomicrographs were taken of the crystal (Figure 15a and b). Some crystals

*Perkin Elmer Model 221 Infrared Spectrometer, Perkin Elmer Mfg., Norwalk, Conn.

3434

Figure 14 TRANSPARENT MgO

TABLE VIII

NiO PREPARATIONS

Run No.	Pressure (psi)	Temperature (°C)	Power (watts)	Time (min)	Results
17	250,000	910	1271	10	Very poor
14	250,000	890	1316	12	Good
11	250,000	940	1390	8	Good
27	250,000	980*	1586	9	Good 728 KHN 100 gram load
23	250,000	980	1592	10	Good (Al_2O_3 contamination)
22	250,000	(1300)*	1785	10	KHN of 800 for 100 gram load
18	500,000	(1000)*	1656	2	Very poor
32	500,000	1000	1664	10	NiO crystals

*Open thermocouple, temperature obtained by interpolation of power versus temperature plots of other runs.

(A)

(B)

3356B

Figure 15 NiO SINGLE CRYSTALS

had growth pits which resembled herring bone (Figure 15b). Some of the crystals were octahedra several tenths of a millimeter in size. Most, however, were of the order of 10 to 50 microns on an edge. X-ray diffraction of one of the octahedra showed it to be a single crystal. Electron diffraction showed the presence of a surface layer of nickel hyroxide resulting probably either from exposure to air or from water pickup during preparation for the diffraction studies.

Samples 27 and 22 pressed at 250, 000 psi at temperatures of 1300° C and 1000° C respectively, showed Knoop hardness values of 728 and 800, respectively. Single crystal NiO has a hardness of 500 KHN.

c. Cr_2O_3

Six runs were made with Cr_2O_3 as shown in Table IX. In general, these did not yield as good specimens as had the other materials. The specimens were very friable and had low density. Often, upon opening the chamber a pronounced odor of H_2S was noticed. This indicated that the decomposition of the sulfate left sulfur as an impurity which reacted with the water from the pyrophyllite to give a vapor phase of H_2S during pressing. One specimen, however, pressed at 1400° C and 250, 000 psi had a fair structure and gave a Knoop hardness of 1570 under a 500 gram load. Upon retest with a 100 gram load the hardness was 1100.

d. Al_2O_3

Linde B alumina is a mixture of γ-alumina, 0.02 micron grain size, and α-alumina, 0.20 micron grain size. The as-received material was preheated to 1000° C to drive off any volatiles and then isostatically cold pressed at approximately 20, 000 psi and again at 38, 000 psi to a green density of about 58 percent theoretical density.

The prepressed Linde B alumina was placed into the high-pressure apparatus with a Pt-Pt+10 percent Rh thermocouple, and pressed at 12.5 kilobars for approximately 30 minutes at temperatures of 500° to 1950° C.

The lower temperature experiments yielded a sample containing two distinct areas (Figure 16). The dark area formed almost a perfect cylinder inside of the deformed area. The deformed area next to the heater was white and porous as compared to the grey area which was more dense. The white area contained γ and α alumina. The grey contained only α-alumina. The higher temperature experiments conducted near 1000° C yielded samples which were very dense and had a Knoop hardness of 2200 to 2300 with a 100-gram load (Figure 17). The resulting grain size was approximately 1 micron for these conditions.

TABLE IX

Cr_2O_3 PREPARATIONS

Run No.	Pressure (psi)	Temperature (° C)	Power (watts)	Time (min)	Results
29	250,000	1230*	1584	6	Fair-good
28	250,000	(1260)*	1607	4	Fair
12	250,000	1400	1680	10	KHN 1571 (500) Fair structure
16	250,000	1580*	1776	3	Poor
15	500,000	940*	1554	10	Very poor
30	500,000	1250	1757	4	Very poor

*Open thermocouple, tmeperature obtained in interpolation of power versus temperature calibration curves.

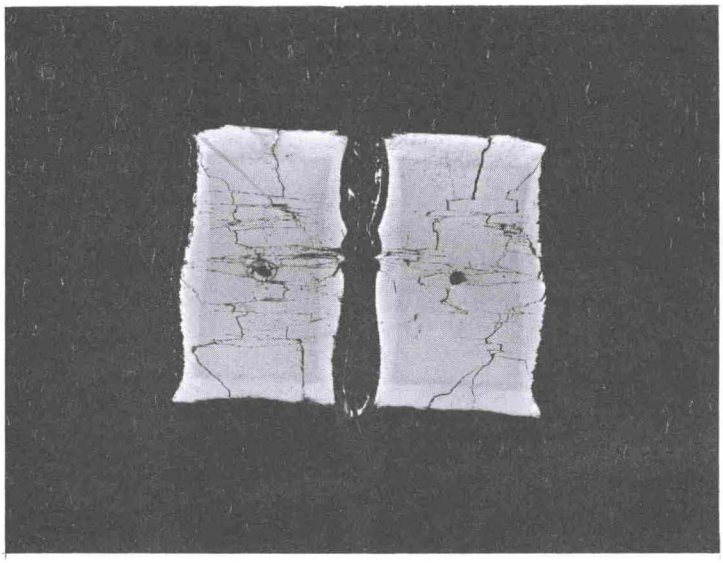

3213

Figure 16 Al_2O_3 SHOWING TWO DIFFERENT AREAS

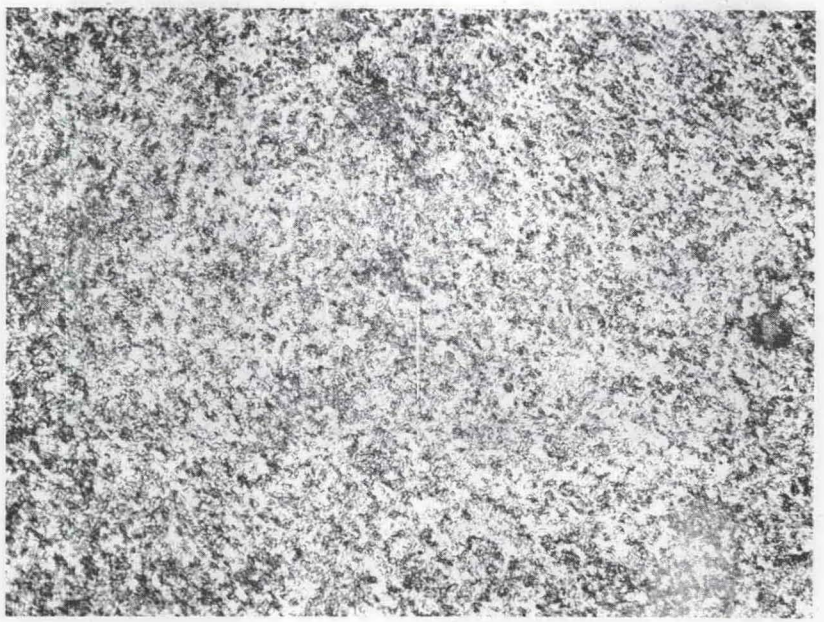

3655

Figure 17 Al_2O_3 MICROGRAPH

4. Delamination of Pressed Specimens

It has been observed that many of the MgO specimens have been severely laminated, giving thin disks from 0.030 to 0.125-inch thick upon removal of the nickel heater sleeve. It is believed that this delamination resulted from elastic recovery during the unloading from the high-pressure condition. The lower elastic limit of the nickel sleeve resulted in its being under axial compression and the MgO under axial tension after the release of pressure. An approximate calculation of the tension on the MgO may be made. Before unloading, the system is in equilibrium at some pressure P_{max}. Upon unloading, with no restraints, the nickel sleeve will expand by an amount

$$\Delta \ln L = \frac{1}{E} \frac{\Delta F}{A} \tag{4}$$

where:

- L is the length
- E is Young's modulus
- ΔF is the change in force on the sleeve
- A is the cross-sectional area of the sleeve.

Using the subscript 1 for MgO and 2 for the nickel sleeve we have, since upon unloading both the sleeve and MgO expand by the same amount,

$$\Delta \ln L = \frac{1}{E} \frac{\Delta F_1}{A_1} = \frac{1}{E_2} \frac{\Delta F_2}{A_2} \tag{5}$$

but,

$$\frac{\Delta F_1}{A_1} = P_{max} - P_{1,\,final} \qquad P_{max} - P_{1,\,final} \qquad \text{(a)} \tag{6}$$

and,

$$\frac{\Delta F_2}{A_2} = P_{max} - P_{2,\,final} \qquad P_{max} - P_{1,\,final} \qquad \text{(b)}$$

However, after unloading, the force on the nickel must be equal and opposite to that on the MgO so that

$$A_1 P_{1,\,final} = -A_2 , P_{2,\,final} \tag{7}$$

Substituting Equations (6) and (7) into (5) we obtain

$$P_{1,\,final} = P_{max} \frac{(E_2 - E_1)}{(E_2 + \frac{A_1}{A_2} E_1)} \tag{8}$$

$P_{1,\,final}$ will be negative (that is the MgO will be under tension) if E_1 is greater than E_2. Typical values of E are 45 x 10^6 psi for MgO[21] and 30 x 10^6 psi for nickel[22].

At the end of the run, the diameter of the sample is about 0.375 inch and the nickel sleeve has a thickness of at least 0.010 inch. The area then is given by

$$\frac{A_1}{A_2} = \frac{\pi\,(0.187)^2}{2\pi\,(0.187)\,(0.010)} = 9.3\,. \tag{9}$$

Substituting these values and P_{max} = 250, 000 psi into Equation (5) we obtain

$$P_{1,\,final} = 250{,}000\ \frac{(30 - 45)}{30 + (9 \times 45)}$$

$$= \frac{15}{435} \times 250{,}000 \tag{10}$$

$$= -8600 \text{ psi}$$

The ultimate tensile strength of a typical dense fine-grain MgO is of the order of 15, 000 to 18, 000 psi.[23] Thus this simple calculation shows a tensile force of about one-half of the strength of the material. The nickel tube deforms severely during the pressing operation, developing transverse wrinkles which (1) provide good contact with the MgO for the transmission of axial forces, (2) possibly introduce stress risers in the MgO at these wrinkles, and (3) may, by changing the area ratio, lead to higher local stresses.

If this model represents correctly the reason for delamination of the specimens, such delaminations may be avoided by:

a. choosing a sleeve material with a higher Young's modulus,

b. using a thinner or weaker sleeve, and/or

c. controlling the delamination by the introduction of shims.

Using the second suggestion a graphite sleeve was used as a heater. The resultant load applied to this graphite sleeve compresses the sleeve as well as the sample without breaking the electrical current. The collapsing of the tube did not increase the internal stresses as was the case for the nickel tubes. This was later proven when large intact pieces were obtained using the graphite sleeve.

IV. COMPRESSIBILITY MEASUREMENTS AT HIGH PRESSURE

A. DYNAMICS MEASUREMENTS -- SOUND VELOCITY STUDIES

1. Introduction

Newton showed that the velocity, v, of a compressional wave in a fluid (sustaining no shear traction) could be expressed as

$$v = \sqrt{\frac{K}{\rho}} \tag{11}$$

where K is the bulk modulus $-v\left(\frac{\partial P}{\partial V}\right)$ and ρ is the density. Laplace showed that the partial $\frac{\partial \rho}{\partial V}$ was at constant entropy $\left(\frac{\partial P}{\partial V}\right)_S$ rather than at constant temperature $\left(\frac{\partial \rho}{\partial V}\right)_T$ as assumed by Newton. The difference between the two, although significant in the case of gases, is small for liquids and solids given by

$$\beta_T - \beta_S = \frac{\alpha^2 VT}{C_V} \tag{12}$$

where

$\beta_T = -\frac{1}{V}\left(\frac{\partial V}{\partial \rho}\right)_T$, $\beta_S = -\left(\frac{\partial V}{\partial \rho}\right)_S$ α is the expansibility, $\frac{1}{V}\left(\frac{\partial V}{\partial T}\right)_\rho$, V is the volume and c_v is the specific heat at constant volume.

In a solid (or any material sustaining shear traction) where both the bulk compressibility $\beta = 1/K$ and the shear modulus μ are finite, both compressional and shear modes of vibration may be propagated with different velocities v_c and v_s respectively given by

$$v_c = \sqrt{\frac{K + 4/3\,\mu}{\rho}} \tag{a}$$

and

$$v_s = \sqrt{\mu/\rho} \ . \tag{b}$$

(13)

In this case, determination of the two velocities v_c and v_s allows the determination of K_S and hence very nearly K_T. Then if v is known, the equations of state may be known to at least two terms in the pressure. If the pressure dependance of K is known, then more terms in the equation of state are available.

Birch[24, 25, 26] has determined the velocity of compressional waves at pressures to 100 kilobars in a large number of minerals and rocks. His two

papers in 1960 and 1961[26] give perhaps the best summary of the information available at that time in addition to his own measurements of some tens of rocks including granites, basalts, dunite, sandstones, linestones, etc.

His measurements were made in an essentially ideal hydrostatic environment. The sample was enclosed in a soft metallic or elastiomeric jacket to exclude the hydraulic fluid. Two transducers, a transmitter and a receiver, were used at opposite ends of a cylindrical specimen, operating through the jacket, for determination of the velocity of the compressional wave.

Simmons[27, 28] modified Birch's apparatus by enclosing the transducer within the jacket and was able thus to generate with AC-cut quartz crystals essentially pure shear waves with a minimum of compressional component. He has reported both compressional and shear velocities for 20 minerals and rocks. In addition Hughes [29, 30] using a similar apparatus has measured the velocity of sound in a number of rocks and minerals.

McSkimmin on the other hand, has an essentially interferometric method.[31, 32] Actually, it is a phase comparison method. An oscillator running at about 10 MHz is gated for pulses and a higher harmonic (about 60 MHz) is used to drive a quartz transducer sealed to the specimen. Phase contract is achieved by overlapping successive reflected pulses on an oscilloscope and observing the frequencies at which addition (or cancellation) occurs. Anderson has used this apparatus for the study of fused silica to 10 kilobars.[33]

Katz used essentially the same technique for measurement, but he achieved higher pressures up to 40 kilobars by pressing the sample between Bridgman anvils. He kept his transducers outside of the high-pressure environment by mounting them in a recess of the piston cap at the other end of the carbide punch.

2. Experimental Methods Proposed

a. Sample Configuration

An attempt was made to extend the pressure range by making measurements within the belt-type apparatus, shown in Figure 1. Initial experiments were to be performed with the 1×10^6 psi (66 kilobars) apparatus and the die-body dimensions used in the previous work. This die body can be opened up to allow the use of larger specimens (1.75-inch pressure) at lower pressures (30 kilobars). The 3×10^6 psi (200 kilobars) apparatus described above provides a sample diameter of 0.5 inch, but, can similarly be opened up to allow operation to 50 kilobars in a volume of approximately 1 inch in diameter and 1 inch in length.

Figure 18 shows the sample configuration in more detail. The quartz tranducer, either X or Y (or AC) cut for compressional or shear excitation, respectively, is mounted on the face of the punch. Lateral support is given by rings of hot-pressed MgO or Al_2O_3. An evaporated coating of platinum or gold on the face of the transducer allows electrical contact to the punch face (RF ground) on one side and to the RF lead on the other side. The sample, either jacketed or unjacketed is located between the punches. Lava (pyrophyllite) gasketing completes the cell.

b. Modes of Operation

Several modes of operation are available as detailed in the next section.

The primary method for obtaining shear and bulk data for materials is by measuring ultrasonic shear and longitudinal wave velocities in the materials when they are in the prescribed environments. There are several method used to accurately measure the ultrasonic shear and longitudinal wave velocities in small specimens. This is because no one method is satisfactory for all cases. Among the factors which affect the selection of a method for any particular case are the accuracy desired; the ultrasonic attenuation of the material; the configuration of the material, and the associated equipment used to cause the desired environmental conditions; and the ingenuity of the investigator.

Some of the standard methods used for measuring ultrasonic velocities in test specimens are described herein along with their limitations. Most of these techniques are either the work of, or derived from, the work of H.J. McSkimmin, of the Bell Telephone Laboratories. Each of the methods described requires an accurate measurement of the specimen thickness which may be done mechanically and the time required for an ultrasonic wave to propagate through the specimen.

1) Method 1 -- Pulse-Echo, Phase Comparison -- This method may be used for either X- or Y- cut crystals when the material being evaluated does not attenuate the ultrasonic wave rapidly. The block diagram is shown as Figure 19.

The oscillator operates continuously and some harmonic, for example the fifth, is selected from each of the harmonic generators. The transducer is driven by short pulses from the gated harmonic generator. If the attenuation of the ultrasonic wave in the specimen is low enough many reflections of the wave will take place. A short pulse length will allow each of these reflections to be clearly distinguished after the initial driving has dissipated. These reflected signals are then fed through some associated circuitry and into an oscilloscope and the time between successive reflections

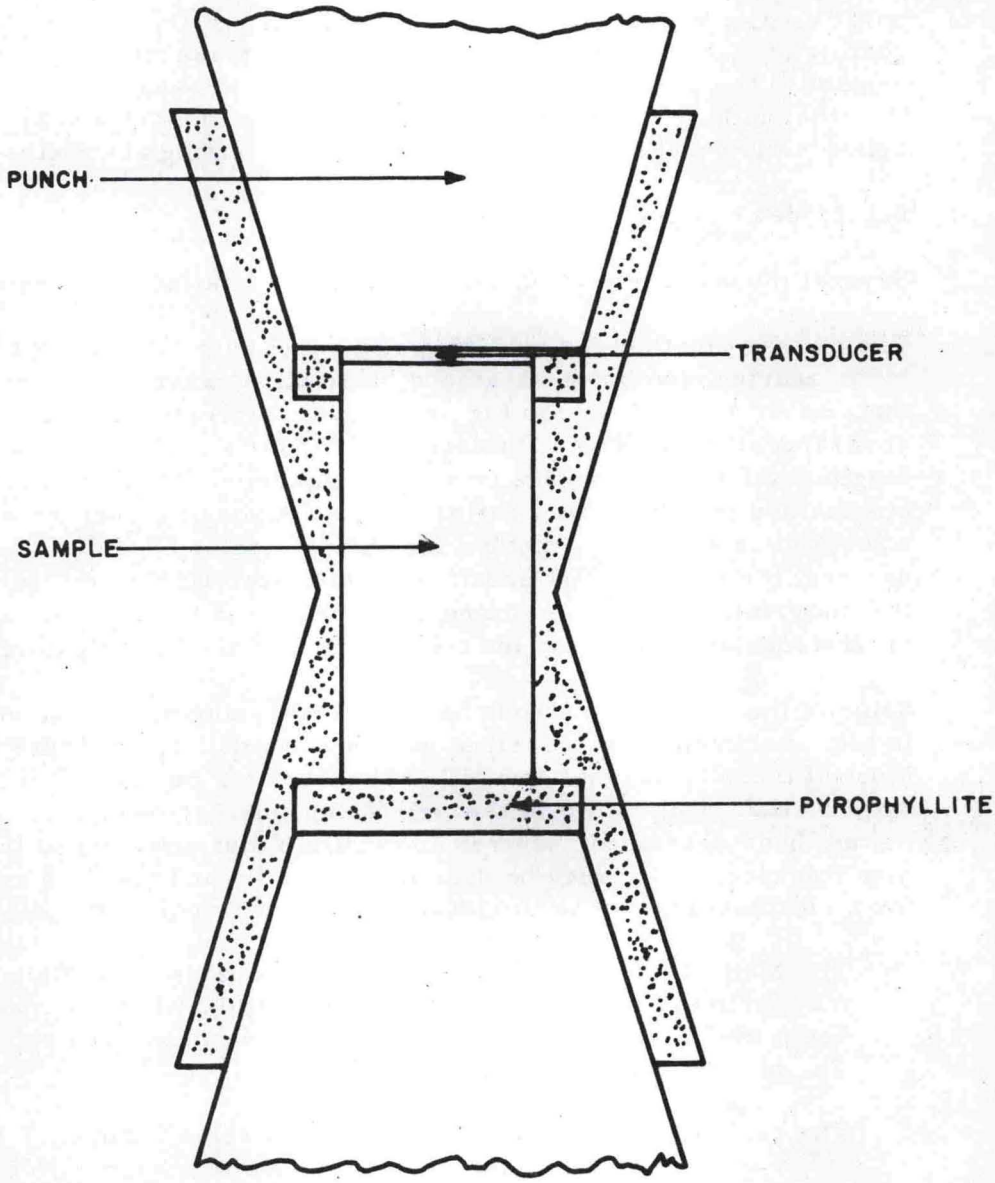

Figure 18 SAMPLE DETAIL

may be determined directly. A low level continuous wave from the other harmonic generator can be superimposed on the reflected pulses. Then the frequency can be varied until the reflected pulses can be varied until the reflected pulses move up and down in unison when the phase (delay) of the low level continuous wave is varied. This will mean that the path is an integral number of wavelengths at the frequency being employed. A measurement of this frequency will give an accurate measure of the velocity of wave propagation.

2) Method 2 -- Phase Comparison -- A second method is a special phase comparison technique for relatively high attenuating materials where only two or three echoes of the ultrasonic signal can be observed. The block diagram is shown as Figure 20.

For this method, two similar pulses are propagated in the material through an appropriate delay so that the driving signals will not interfere with the reflected signals. Initially, both signals are applied simultaneously, then the phase of amplitude of one is adjusted slightly for complete cancellation of the first echo reflected from the back of the test specimen. Gate 2 is opened later than gate 1 so that the first reflection from the second gate lines up with the second echo from the first gate. The frequency is then adjusted until phase cancellation takes place between these two reflections and each of the subsequent pairs. At this frequency, the path length will be an odd number of half wavelengths and an accurate velocity determination can be obtained when the frequency is known.

3) Method 3 -- Modified Phase Cancellation -- The third method is a modification of the first technique discussed. It appears that it would be easier to implement than the first technique for materials which do not attenuate the ultrasonic signal excessively. The block diagram is shown as Figure 21.

The transducer is placed on the test specimen and driven by a wave train which is approximately three times the length of the test specimen in that material. This causes the last one third of any given wave train to be adjusted until phase cancellation or addition takes place for each of these successive reflections where the signals overlap. The time between reflections which can be obtained from the oscilloscope display and knowledge of frequency being used permit an accurate determination of the transit time of the ultrasonic pulse.

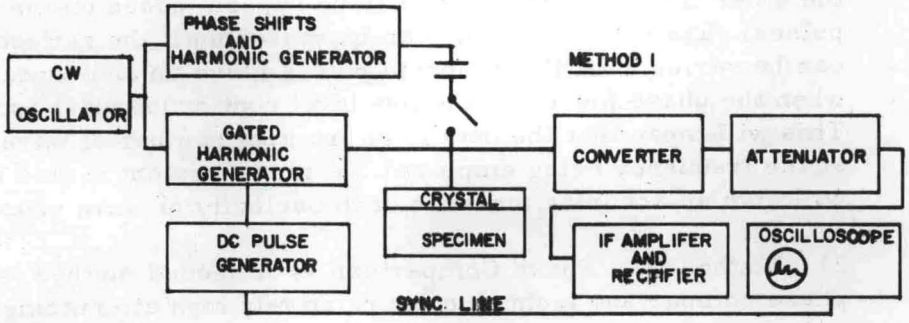

Figure 19 BLOCK DIAGRAM FOR PULSE-ECHO PHASE COMPARISON MODE

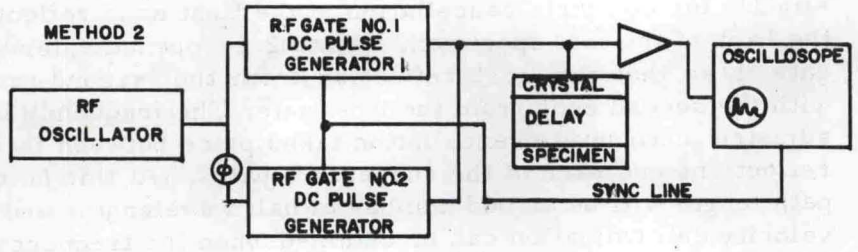

Figure 20 BLOCK DIAGRAM FOR PULSE-ECHO PHASE COMPARISON MODE

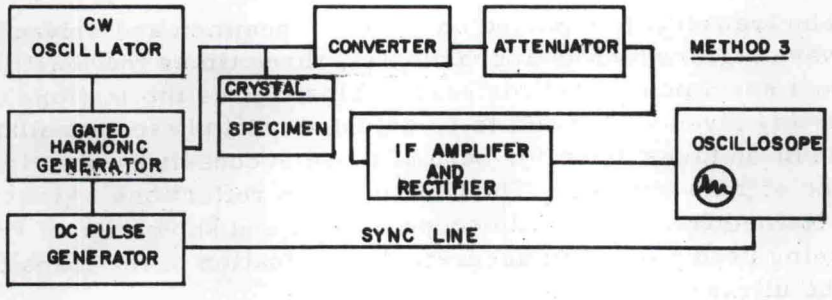

Figure 21 BLOCK DIAGRAM FOR MODIFIED PHASE CANCELLATION MODE

4) Method 4--Through Transmission Technique -- There are several variations of this technique. They all require that two crystals can be used, one on each side of the specimen and in addition a comparison signal may or may not be sent through a delay network parallel to the specimen under test. The particular procedure being used depends on the attenuation of the ultrasonic signal in the specimen at the frequency being employed. If the attenuation is low, then the setup shown below may be employed. (See Figure 22.)

A long wave train is used to drive the transmitting transducer. The frequency of the oscillator is varied until each reflection in the test specimen either constructively or destructively interfered with the subsequent reflection. A measurement of the frequency will then allow an accurate measurement of transit time.

If the attenuation in the material is very high, an accurate measurement of transit time can be made by coupling two transducers directly to the material and transmitting an ultrasonic signal directly through it. The accuracy of this method for velocity measurement increases with the length of the specimen and may be improved by comparing with the transit time in some well-known standards.

5) Method 5--Resonance Techniques -- Another method that may be used when the material being evaluated does not attenuate the ultrasonic signal excessively is the resonance method, as shown in Figure 23. For this method, the crystal is driven by a continuous wave and the frequency of this wave is varied. At the resonant frequency of the test specimen, or harmonics of this frequency, there will be an increase in the amplitude of the waves in the material that is, when the wave reflected from the back surface of the test specimen arrives at the crystal with the same phase as the transmittal signal. A measurement of the plate current of the output tube will allow one to determine when the resonant condition and its associated change in crystal loading occurs. The frequencies at which resonance occurs is accurately measured with a frequency counter. The resonant frequency may be used to determine the velocity of the wave in the material by using any of several methods for determining which harmonic a given resonant frequency represents.

3. Experiments

In preparation of the sound velocity measurements that were conducted in the high-pressure apparatus, feasibility studies were initiated using a quartz crystal.

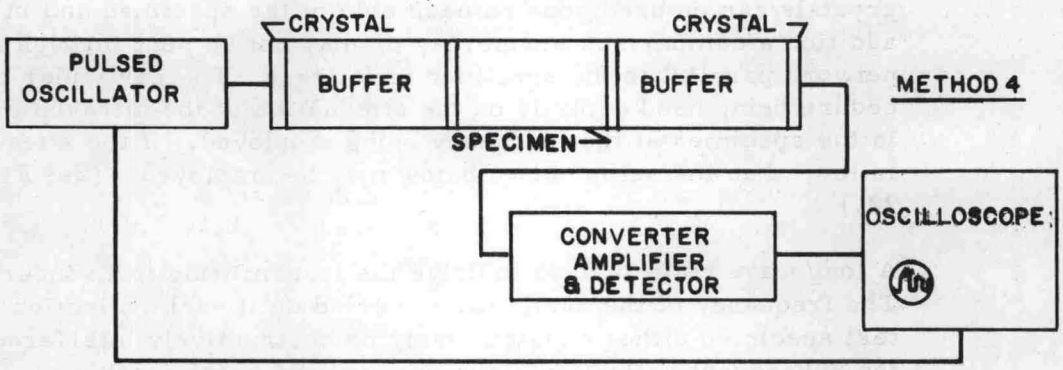

Figure 22 BLOCK DIAGRAM FOR THROUGH TRANSMISSION

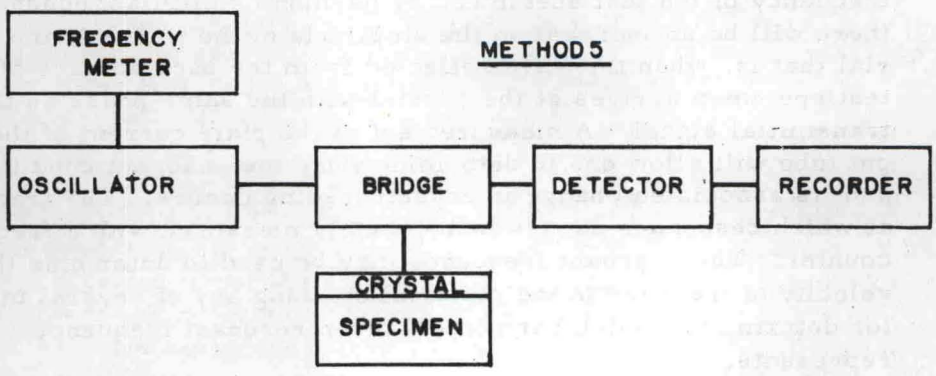

Figure 23 BLOCK DIAGRAM FOR RESONANCE TECHNIQUES

This quartz crystal was placed between the punch and the sample as shown in Figure 18. Only one crystal was used in our preliminary investigation. The first experiment conducted using one crystal was quite successful. Very little cracking occurred in the quartz crystal. The cracks that formed were due to the collapse of the pyrophyllite disc which was located at the other end of the sample as shown in Figure 18. When the pyrophyllite collapsed, a shock wave traveled through the sample and cracked the crystal.

The sample mounting was modified, as shown in Figure 24, so that the load was on the crystal and the sample and not in the pyrophyllite. The punches were broken and the quartz transducer was crushed. It is believed that this failure was initiated by undetected cracks in the punches and/or in the sample. Additional punches used for these measurements were plated with nickel to decrease the contact resistance between the transducer and the punches.

The assembly of the sample was modified and the transducers were modified as shown in Figure 25. The transducers were placed between the punch and a piece of aluminum foil. Silicone grease or Vaseline was rubbed on both sides of the aluminum disc. This was done to assure coupling of the transducer with the sample. The sample used in this experiment was Stupalox; doped alumina.

In the first attempt, at atmospheric pressure, quartz crystals, vapor plated with gold, were used as the transducers. Using a 3-MHz pulse generator, no signal was detected in the sample. Another attempt was made with X-cut 3-MHz quartz crystals, and again, no signal was detected. Therefore, a dummy assembly was made using the same sample material and quartz crystals. It was found that with the 3-MHz pulse generator, the quartz crystals could not be activated, and lead zirconate crystals (silver plated on each side) were substituted for quartz. Electrical contact was made at one side directly to the tungsten carbide punch and at the other side to the aluminum foil which was brought out through the pyrophyllite insulation. Mica rings surrounded the transducer crystal provided lateral support as shown in Figure 25.

The instrumentation used for this assembly is illustrated in Figure 26. A piece of copper 0.750 inch x 0.750 inch x 0.500 inch was used as a velocity standard. The velocity of sound through this reference standard was determined to be 0.128 inch per μ sec, while the sound velocity for the Stupalox specimen was 0.401 inch per μ sec, at 1 atmosphere pressure. As the pressure was increased very slowly on the specimen, the signal through the crystals was lost. The signal could neither be received nor transmitted into the Stupalox. The reference standard was operating properly, but a resistance check of the sample indicated a short between punch face and the aluminum disk. Therefore, the press was opened and transducer examined in place. The mica insulation rings had compressed so badly that the full load was on the crystal. This shattered the crystals and shorted the aluminum leads to the punch assembly.

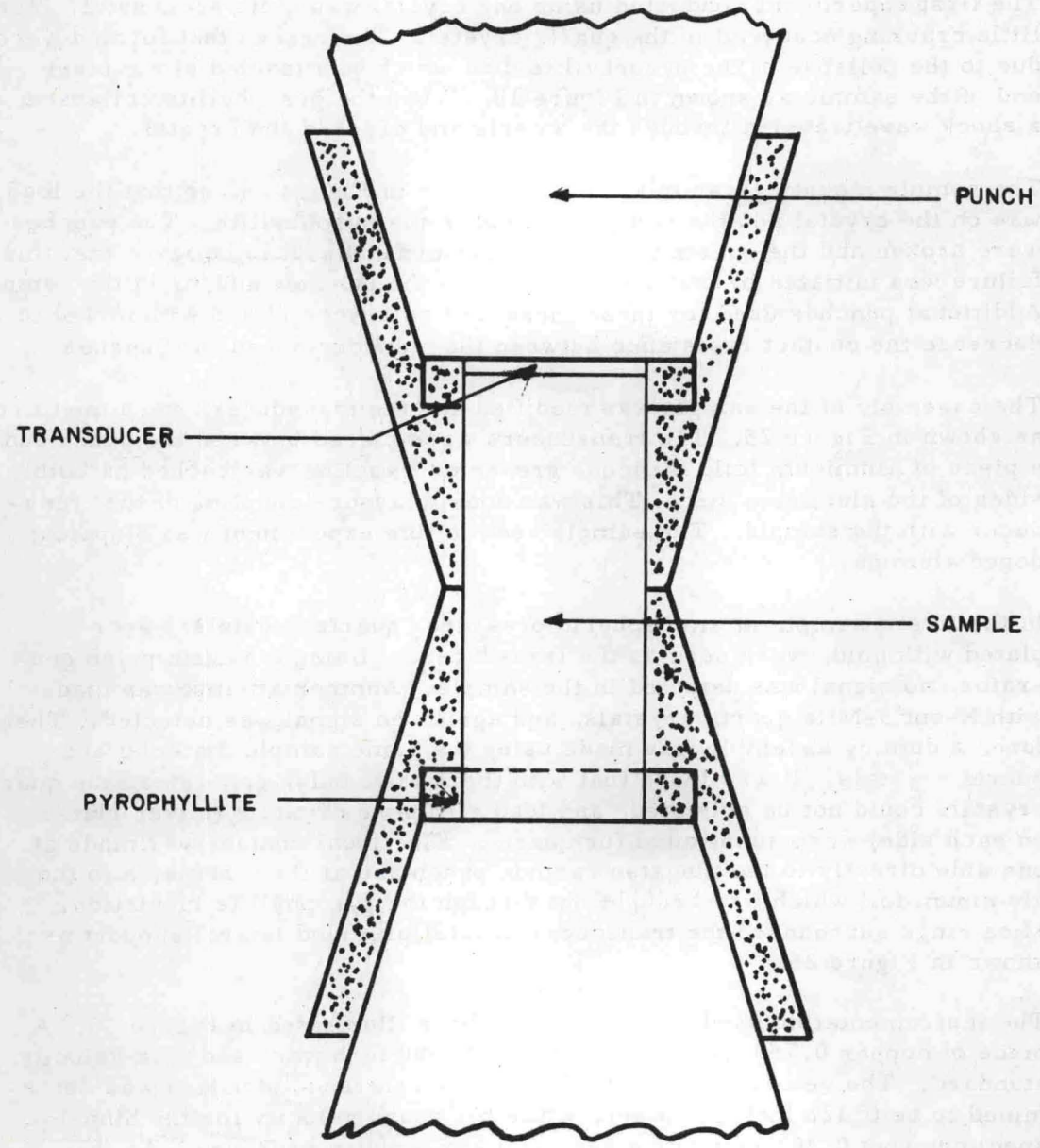

Figure 24 SAMPLE DETAIL PRELIMINARY TESTS

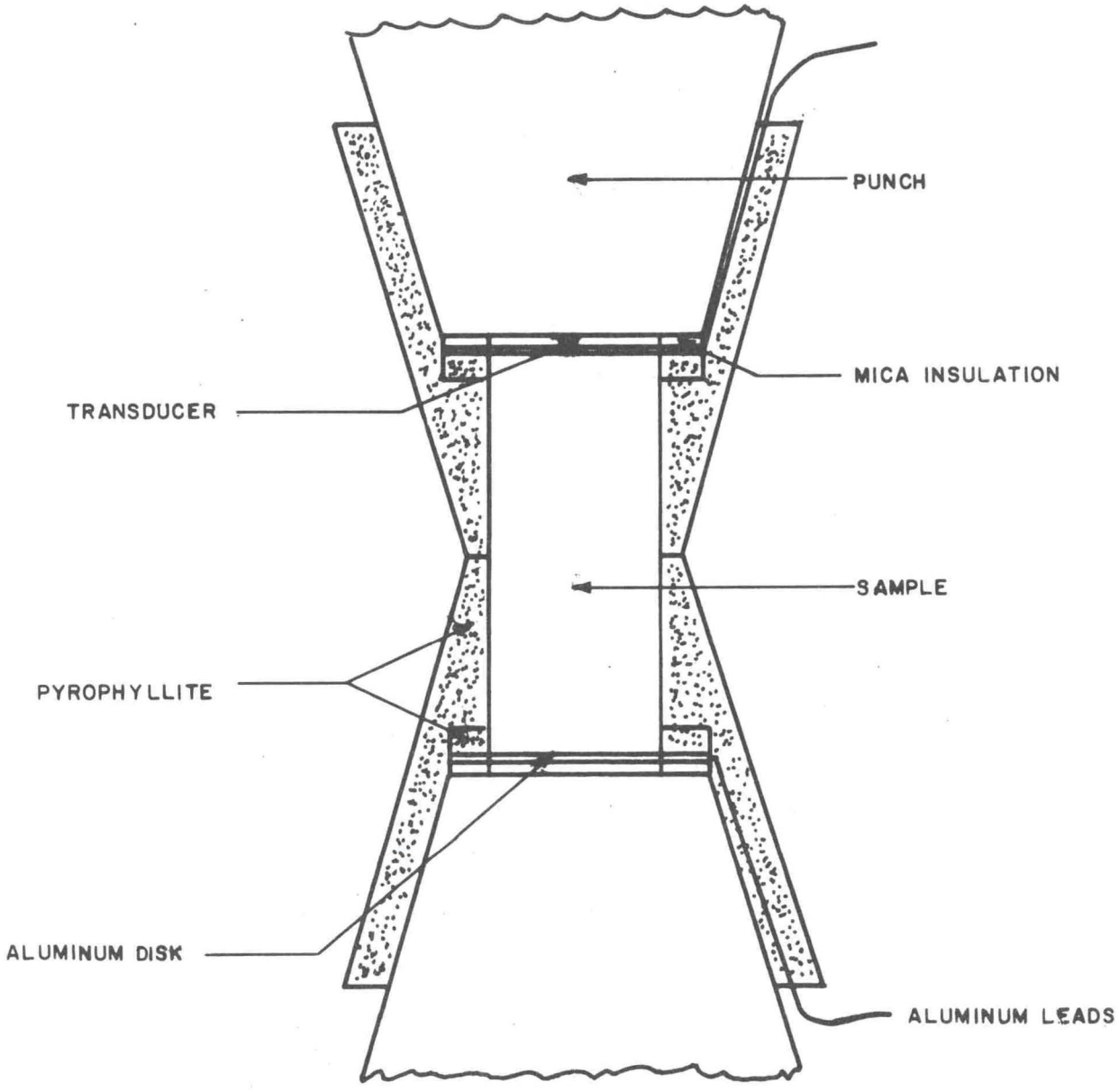

Figure 25 SAMPLE DETAIL PRELIMINARY TESTS

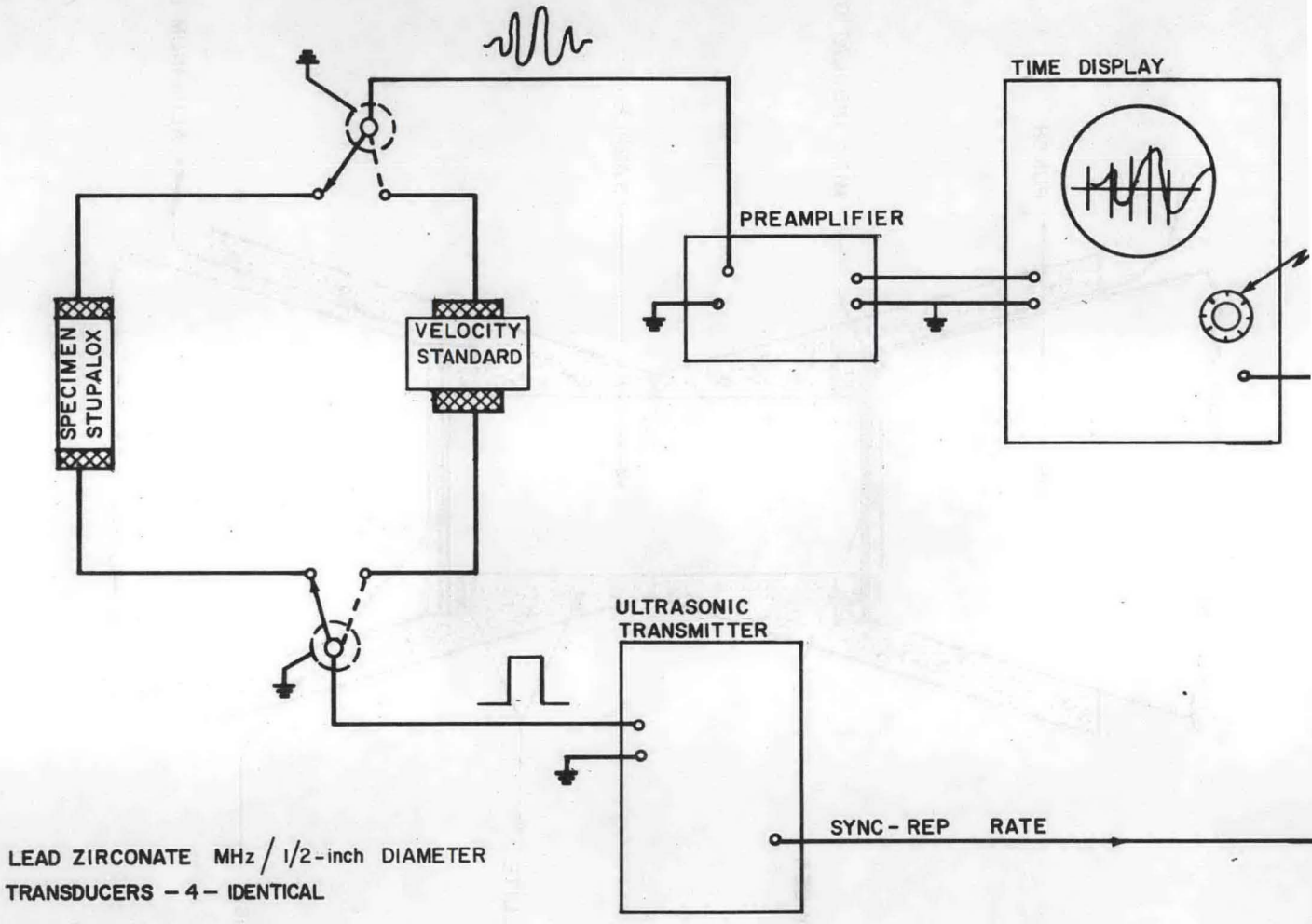

Figure 26 INSTRUMENTATION FOR SOUND VELOCITY STUDIES

B. STATIC MEASUREMENTS -- X-ray STUDIES

1. Introduction

High pressure X-ray diffraction studies have been performed with a camera similar to that described by Mariano. In this camera, high pressure is achieved between diamond anvils. A collimated beam is brought through one diamond. The diffracted rays fan out through the other diamond and infringe on a flat photographic plate of film. The apparatus is shown in Figure 27 and in Figure 28.

With powder specimens, Debye rings are formed and the interplanar spacing d may be calculated from the formula

$$d = \frac{\lambda}{\sqrt{2}\left[1-\left(\frac{1}{1+x^2}\right)^{1/2}\right]^{1/2}} \qquad (14)$$

where λ is the wavelength of the radiation employed and x is the ratio of the measured radius of the Debye ring to the sample-to-film distance.

The compressibility β_T is defined as $-(1/V)(\partial V/\partial P)_T$ where V is the volumen, P, is the pressure and T is the temperature, but this is just three times the linear dilatation $(1/d)(\partial d/\partial p)$ where d is an interplanar spacing. Differentiating the expression given earlier we can obtain

$$\beta = \frac{3x(\partial x/\partial p)}{2(1+x^2)[(1+x^2)^{1/2}-1]} \qquad (a)$$

or for finite changes (15)

$$\beta_{av} = \frac{3x(\Delta x/\Delta p)}{2(1+x^2)[(1+x^2)^{1/2}-1]} \qquad (b)$$

2. Experimental Techniques

To measure the compressibility we measure the line shift observed between exposure at different pressures. By superinforcing exposures at different pressures on the same film, errors due to changes in the sample-to-film distance or film shrinkage, etc. are avoided. The line displacement which is proportional to the compressibility is easily estimated to one-twentieth of a millimeter. Attempts have been made to resolve the shifted lines with a densitometer in order to achieve even greater precision. However, at convenient exposure levels this could not be done.

15512 B

Figure 27 EXPLODED VIEW OF HIGH PRESSURE X-RAY CAMERA

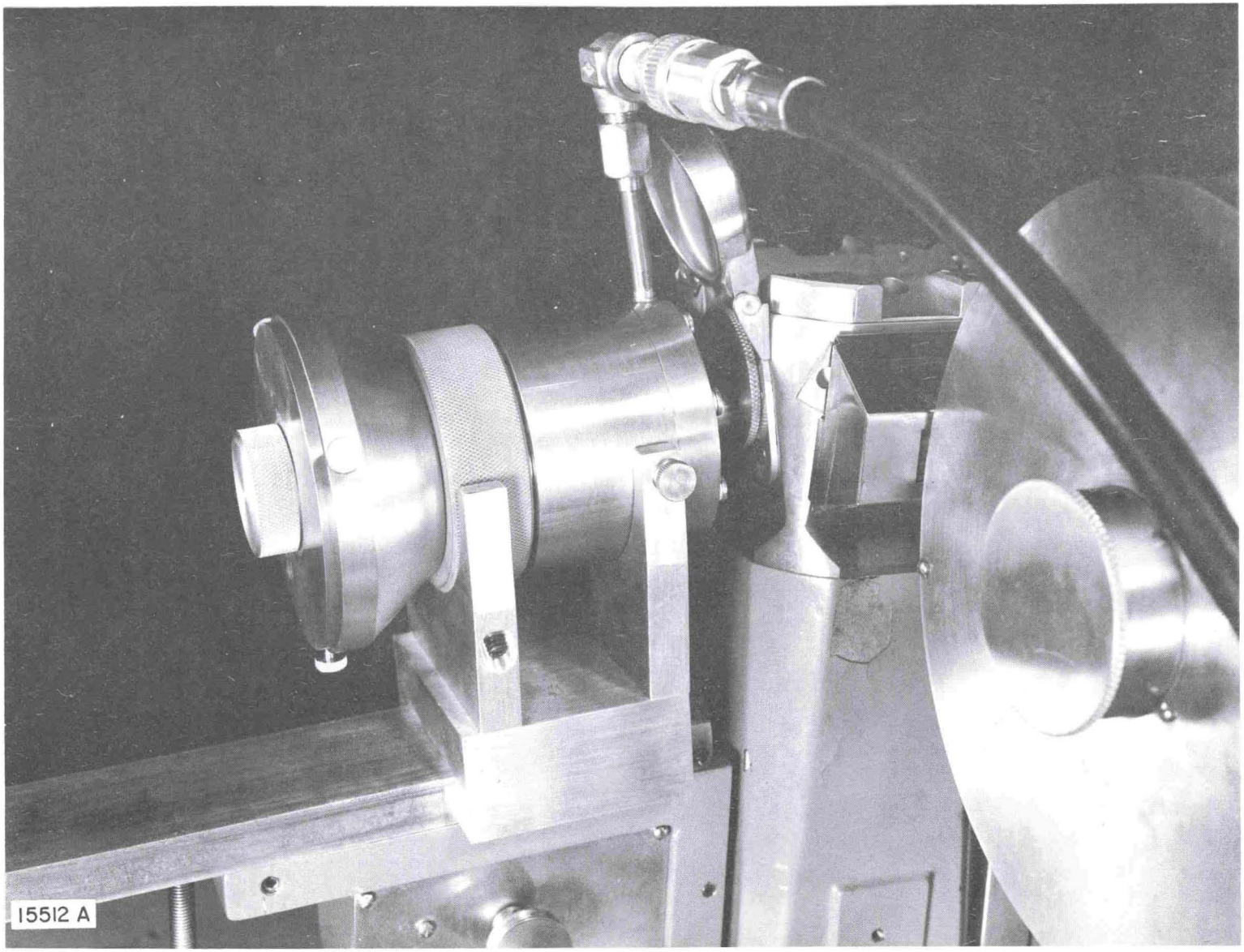

Figure 28 HIGH-PRESSURE CAMERA INSTALLED

Extrusion of the sample from between the faces of the diamond anvils results in a loss in intensity of the diffraction rings and, if extensive, in a reduction in pressure under the anvils by filling the space around the anvils, and absorbing some of the load. Powder samples have been prepared in several ways to avoid this difficulty. The best samples have been prepared by prepressing at about 1000 psi either dry powders or powders which have been infiltrated with parlodion.

Before pressing, a copper specimen support 2-1/2 mm in diameter with a 0.8-mm central hole is placed on the powder. During pressing the powder is forced into this hole. The excess powder is trimmed away and the sample is mounted between the diamond anvils. This copper ring gives lateral support to the sample.

Typical photographs are shown in Figures 29 and 30. This sample material is rubidium chloride. The first figure showns two exposures at 25 kilobars and at 1 atmosphere. Lines are observed of both the high-pressure form with the cesium chloride and the low-pressure form with the rock salt structure. Also visible are Laue spots from the two diamond crystals.

A complete list of the exposures made to data are given in Appendix B. The X-ray camera furnished by the manufacturer was supplied with two pistons. On one of these the punch diamond was rigidly fixed to the face of the piston. On the other the punch diamond was mounted on an insert which swiveled on a spherical bearing attached to the piston. In theory, this would facilitate the alignment of the diamond faces. However, in practice this mounting allowed the punch diamond to contact the anvil diamond at random positions. At the conclusion of a run, the punch diamond was found completely off the anvil diamond in at least one case. Although in each case initial contact between the diamonds was made with the axis vertical and a slight holding pressure was maintained after rotation to the horizontal, the weight of the self-aligning mount allowed the punch to drop out of position. Therefore, in all runs after No. 15, the fixed mount was used.

Diamond failures in this program have been infrequent although replacement deliveries have occasionally slowed the program. Only one failure of the punch diamond was observed. After preliminary runs, it was found that the height of the original punch diamond was less than the thickness of its mounting plate. On the first application of pressure, this diamond was pushed out of its mount. A new mounting plate was fabricated to allow 0.007-inch clearance. On the run subsequent to No. 17, a crack was heard as the pressure was being raised. Upon examination the punch diamond was found cracked on (111) planes with a small pyramidal piece broken out of the center. The replacement diamond was used as received until run 41. To allow more room around the diamonds and prevent transference of the load through the sample to the mounting plate, the diamond was remounted with the

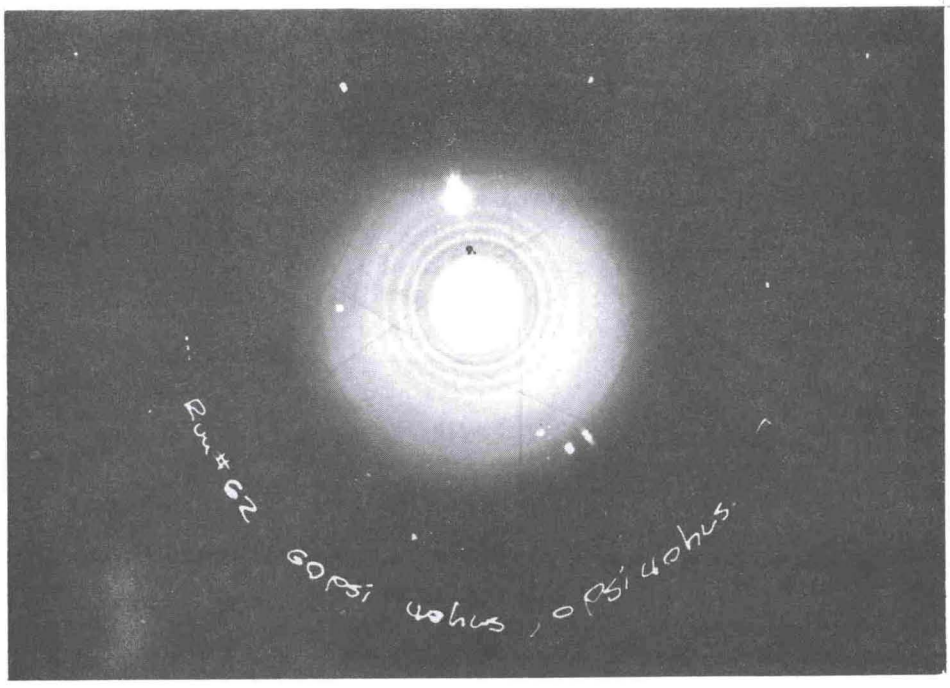

Figure 29 X-RAY PATTERN OF RbCl at 1 BAR AND 25 KILOBARS

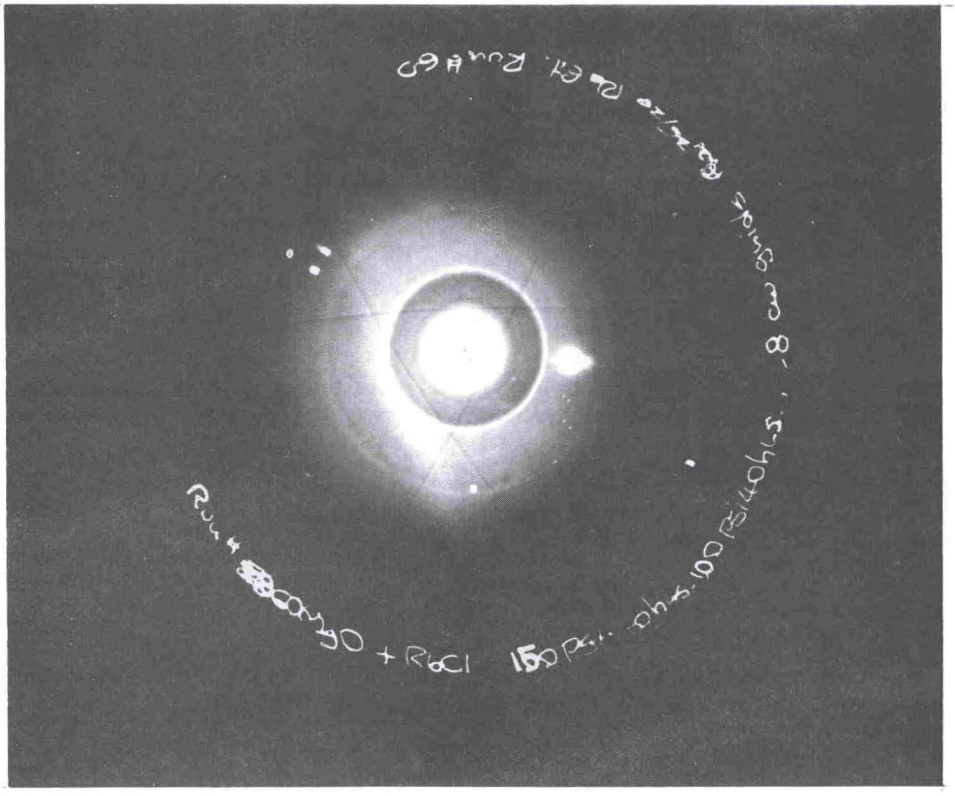

Figure 30 X-RAY PATTERN OF RbCl AT 40 AND 60 KILOBARS

retaining plate flush against the piston face. After run 133, this diamond was removed and inspected for alignment of the core axis with the pressing direction in hopes that it might be substituted for the anvil diamond. However, the alignment was not good and it was replaced in position on the piston.

The punch diamond, being supported over the whole area of its surface by the piston face except for the beam hole, is subjected to much less severe stresses than the anvil diamond which is supported only on its conical surface More failures have been observed in this diamond.

The first anvil diamond was used without change for 71 runs. Upon raising the pressure for run 72, a noise was heard in the cell. Upon inspection, it was found that the anvil diamond had not been mounted in the plate itself, but had been mounted in an approximately 0.0250-inch-diameter steel insert which had slipped about 1 mm under load. The plate was pressed out and the plate containing a spare mounted diamond was pressed in. On the first application of pressure this diamond cracked. The original unbroken diamond was sent back to be remounted in a new plate. This, after remounting, broke after three runs. The third diamond was removed after five runs because of low table clearance. That is, the height of the table above the mounting plate was insufficient to prevent extruded sample material from assuming part of the load. After remounting in a new plate, this diamond broke on the first application of load. The fourth diamond was used for 14 runs. However, it may have been broken after about 11 of these, judging from the appearance of the films. The fifth diamond was found broken in its mounting plate before use.

The next diamond was used for 19 runs without failure. However, experiments in other laboratories had indicated that brilliant cut gem diamonds, which are actually less expensive than those ground to the conical shape of the original design, were suitable. In the use of brilliant-cut stones, the culet is used as the loading surface. For this application, the culet is made somewhat larger than is normal for a gem. The diamond is supported on its table face. Since the sample is raised above the apex of the 45-degree cone machined in the anvil insert plate, a slot was machined in that plate to allow observation of the diffracted X-ray out to the full angle $2\theta = 45$ degrees originally available. A brilliant-cut diamond in this configuration was used for 20 runs. However, the small size of the culet which was advantageous in achieving high pressure at low load introduced large stress gradients in the volume illuminated by the X-ray beam. The culet diameter was only slightly larger than the X-ray beam itself and the pressure fell nearly to zero within the illuminated volume.

For runs subsequent to No. 133, a brilliant-cut stone has been used mounted in the normal fashion, that is, with the punch diamond bearing on the table of the anvil diamond which in turn is supported by the faces below the girdle. No failures have yet occured with this mounting.

Samples were originally prepared in three ways:

a. By binding with a solution of cellulose acetate in amyl acetate

b. By pressing such a compact at about 8000 psi

c. By pressing dry powders at the same pressure.

Without lateral support of the sample, however, plastic flow during the application of pressure results in such extensive extrusion that little sample thickness is left between the diamond faces. This typically is of the order of a fraction of a mil. Only after very long exposures then an the Debye lines of X-ray photograph clearly visible. Lateral support of the sample was, however, achieved by the use of copper discs approxiamtely 2.3 mm in diameter with a 0.8-mm hole. Such discs are prepared by electrodeposition for use in electron-microscopy sample preparation and are commercially available. Similar discs with a copper grid across the center hole were tested, but were not as effective.

In addition to the loss of sample, the extrusion which occurred in the absence of any lateral support allowed the sample material outside the face of the smaller diamond to take part of the load. This reduced the load on the diamond and hence the pressure achieved in the indicated volume of the sample.

3. Results

a. Rubidium Chloride

Rubidium chloride was mixed 50 percent by volume with MgO. The sample preparation technique was the same as described above for KCl-NaCl. An initial run with a gas pressure of 100 psi was made to check the completeness of the conversion to the high pressure form at the load represented by that gas pressure and to determine exposure time. Run 60 was then made at two values of the gas pressure, 150 psig and 100 psig. Two values ot the compressibility product were obtained from the splitting of the (110) and (200) lines of RbCl-II. These were 0.126 and 0.150 with a mean of 0.138. The MgO with a much lower scattering cross section gave no observable diffraction lines and hence no internal pressure calibration was obtained. After observing the completeness of the reconversion to RbCl-I in run 61, run 62 was made with gas pressures of 60 and 0 psig. Both RbCl-I and RbCl-II lines were observed with no splitting of either indicating that at the higher load only the high-pressure form was present and at the lower load only the low-pressure form.

Run 63 at gas pressures of 40 and 0 psig showed only RbCl-I. Four values of the compressibility product with a mean of 0.124 were obtained. Assuming that the pressure is proportional to the load, the compressibility of the high-pressure form is 5.6×10^{-3} $kbar^{-1}$.

b. Rubidium Bromide

Internal pressure calibration in the rubidium bromides system was difficult. The use of rubidium chloride which had previously been studied was not practicable because the two rubidium salts form a solid solution. Sodium iodide and rubidium bromide metathesize to give sodium bromide and rubidium iodide with the most intense X-ray diffraction from the latter because of its high average Z. Silver gives interferences with both the low-and high-pressure forms. Platinum has a much lower compressibility and splitting could not be observed.

Since internal calibration was difficult, the pressure ratio was calculated from geometry. This indicated an average pressure over the anvils equal to 0.071 kilobar per psi gas pressure. However, a number of runs indicated that the transition previously determined to occur at 6.0 kilobars was observed at a pressure of approximately 10 psi giving a pressure ratio of 0.6 kilobar per psi gas pressure. This gives a ratio of peak-to-average pressure of about 8.5 which is higher than previously observed. Using this calibration, however, and the observed splitting runs 138 and 139 an average value of β equal to 7.1×10^{-3} $kilobar^{-1}$ or 7.1×10^{-12} cm^2 $dyne^{-1}$ was obtained for the high-pressure phase (CsCl structure) of rubidium bromide.

V. CONCLUSIONS AND RECOMMENDATIONS

The high-pressure research studies conducted under this program have been four varieties: Densification of oxides; synthesis of new materials; compressibility measurements, and sound velocity measurements.

The densification studies have shown that completely dense transparent oxides with extremely fine grain size can be prepared at relatively low temperature under ultrahigh pressure.[34, 35, 36] Along with the fine grain size, high hardness values have been obtained,[37] e.g., the hardness of magnesium oxide produced by these techniques was twice that of single crystals of the same oxide and 30 to 50 percent greater than that of hot-pressed material. The processing variables have been studied and optimum conditions found. A series of samples have been prepared and submitted to the Air Force Cambridge Laboratories for further study, in-house, of the relations between hardness and other physical properties. Similar studies of the densification at ultrahigh pressure may lead to improved values of other properties e.g., magnetic permeability or coercive force, or dielectric permittivity or coercive force in appropriate materials. Such studies proposed earlier, but deferred in favor of others should be resumed now.

In experiments with the high-pressure apparatus, the synthesis of the high-pressure modifications of boron nitride (cubic BN) and silica (Coesite) have been duplicated. In addition in studies of the rare earths, a new form of the oxyhydroxide of samarium has been dixcovered and characterized.[38] The systematic study of the oxides and oxyhydroxides of only the rare earth elements would constitute an extensive program of itself. No recommendations are made at this time for continued work along these lines.

X-ray diffraction studies have been performed in a camera in which the high pressure is achieved between diamond anvils. This camera is best suited to the study of phase transformation at high pressure. It has been used for the measurement of the compressibility of the high-pressure modification of alkali halides above their transition pressures. Results have been obtained for the high-pressure forms (cesium chloride structure) of rubidium bromide and rubidium chloride.[39] These studies of compressibility should be continued. In addition, studies of phase transformation per se in compounds of interest to the Electronic Material Sciences Laboratory should be undertaken.

VI. REFERENCES

1. Lonsdale, K., Further Comments on Attempts by H. Moissan, J. B. Hannay, and Sir Charles Parsons to Make Diamonds in the Laboratory, Nature, 196, 104, (1962).

2. Bridgman, Percy W., Physics of High Pressure (London, G. Bell and Sons, Ltd., 1952).

3. ibid p. 189.

4. ibid p. 98.

5. Bridgman, P. W., An Experimental Contribution to the Problem of Diamond Synthesis, J. Chem. Phys. 15 (1947,pp. 92-98).

6. Bridgman, P. W., Compressibilities and Electrical Resistance Under Pressure with Special Reference to Intermetallic Compounds, Proc. Am. Acad. Sci., 70 (1935, pp. 285-317).

7. Bridgman, P. W., Physics of High Pressures (London, G. Bell and Sons, Ltd., 1952) p. 149.

8. Hall, H. T., Ultra-High Pressure, High Temperature Apparatus: the "Belt", Rev. of Scientific Instrument, 31, No. 2 (February 1960) pp. 125-131.

9. Bundy, F. P., H. T. Hall, H. M. Strong, R. H. Wentorf, Jr., Nature, 176, 51 (1955).

10. DeVries, K. L., G. S. Baker, and P. Gibbs, Survey of High Pressure Effects of Solids, WADC Technical Report 59-341 (October 1960).

11. Berg, L., and H. Herman, Literature Survey on Research and Development on High Pressure Technology, WADC Technical Report 59-730 (March 1960).

12. Zeitlin, A., Annotated Bibliography on High Pressure Technology, ASME Publication.

13. Hall, H. T., High Pressure Data Center, P. O. Box 60 University Station, Brigham Young University, Provo, Utah, 84601.

14. Timoshekno, S., Strength of Materials, Part II, Third Edition (New York, D. Van Nostrand Co., Inc., 1956).

15. Kennedy, G. C. and P. N. Lamori, Some Fixed Points on the High Pressure Scale, Pub. No. 195, Institute of Geophysics, University of California.

16. H. M. Strong, and R. E. Hanneman, Pressure Dependence of EMF of Thermocouples to 1300° C and 50 kilobars, ASME 69WA/PT-21.

17. Wentorf, R. H., Jr., Cubic Form of Boron Nitride , J. of Chem. Phys. (26), 4 (April 1959, p. 956).

18. Coes, Loring, Jr., High Pressure Minerals, J. of Am. Ceram. Soc. (38), 8 (August 1955) p. 298.

19. Stishov, S. M., and S. V. Popova, New Dense Polymorphic Modifications of Silica, Geokhimiga 10 (1961) pp. 837-839.

20. Chao, E. C. T., J. J. Fahey, and Janet Littler, "Stishovite", SiO_2 a Very High Pressure New Mineral from Meteor Crater, Arizona, J. of Geophys. Res. (67), 1 (January 1961) p. 419.

21. Chung, Sevica, and Crandall, J. Am. Ceram. Soc., 46 (1963) p. 452.

22. Handbook of Chemistry and Physics, 37 Edition, Chem. Rubber Pub. Co., Cleveland (1955), p. 1985.

23. Spriggs, R.,L. Brissett, and T. Vasilos, J. Am. Ceram. Soc. 46 (1963), p. 508.

24. Birch, Francis, Effect of Pressure on Rigidity of Rocks, J. of Geol. 46 (1938) pp. 59-141.

25. Birch, Elasticity of Igneous Rocks at High Temperature and Pressure, Bull. Geol. Soc. Am. 54 (1943) p. 263.

26. Birch, Velocity of Compressional Waves in Rocks to 10 Kbars, Parts I & II, 65 (1960)p. 1083; 66 (1961) p. 2199.

27. Simmons, G., Velocity of Compressional Waves in Various Minerals at Pressures to 10 Kilobars, J. Geophys. Res., 69 (1964) p. 1117.

28. Simmons, G., Velocity of Shear Waves in Rocks to 10 Kilobars, J. Geophys. Res., 60 (1964) p. 1123.

29. Hughes, D. S., and J. H. Cross, Elastic Wave Velocities at High Pressures and Temperature, J. Geophys. Res. 16 (1951) p. 577.

30. Hughes, D. S., and C. Maurette , Variation of Elastic Wave Velocities in Granite with Pressure and Temperature, J. Geophys. Res., 21 (1956) p. 277.

31. McSkimmin, H. J., Ultrasonic Measurement Techniques Applicable to Small Solid Specimens, J. Acoust. Soc., 22 (1950) p. 413.

32. McSkimmin, H. J., Elastic Moduli of Single Crystal Geranium as a Function of Hydrostatic Pressure, J. Acoust. Soc., 30 (1958) p. 314.

33. Anderson, O. L., "An Accurate Determination of the Equation of State by Ulstrasonic Measurements", Progress in High Pressure Research (New York, John Wiley & Sons, 1961).

34. DeLai, A. J., R. M. Haag, R. M. Spriggs, and T. Vasilos, Ultrahigh Density and Submicron Grain Size Magnesia Prepared by Very High Pressures, (To be submitted) J. Am. Ceram. Soc.

35. Burnett, R., A. J. DeLai, R. Duff, and A. Heuer, Growth Studies in High Pressure Sintered MgO, (paper presented at 3rd International Symposium on Materials, University of California, Berkeley, California (12-16 June 1966).

36. DeLai, A. J., R. M. Haag, and J. K. Hill, High Pressure Preparation and Properties of Polycrystalline Oxides and Halides, paper presented at Basic Science Division, Am. Ceram. Soc., 1965 Fall Meeting at Pittsburgh Pennsylvania.

37. Mansur, F., and J. Plendel, of AFCRL, A. J. DeLai, R. M. Haag, and T. Vasilos, of Avco/SSD, Hardness and Optical Properties of Polycrystalline Oxides (to be published).

38. DeLai, A. J., R.M. Haag, and T. Vasilos, Formation of a New High Pressure Phase of SmOOH (to be submitted).

39. DeLai, A. J., R. M. Haag, and J. K. Hill of Avco/SSD and T. Mansur and J. Plendl of AFCRL, Compressibility of Alkali Halides, (to be published).

APPENDIX A

STRESS ANALYSIS FOR 1 x 10^6 psi APPARATUS

PUNCH ASSEMBLY

A. INSTALLATION OF RING C INTO A AND B (Figure A-1)

During the assembly of A-B, no appreciable stresses are induced since a very small force, if any, is required during its installation. (Ref. Figure A-10.)

Interference between Ring C and Ring A-B assembly is 0.008 inch on the radius. Its contact pressure is given by

$$p = \frac{E\delta}{b} \frac{(b^2 - a^2)\ (c^2 - b^2)}{(2b^2)\ (c^2 - a^2)}$$

$$= \frac{29 \times 10^6 \times 0.008\,(\overline{2.15}^2 - \overline{1.40}^2)(\overline{3.50}^2 - \overline{2.15}^2)}{2.15\ (2)\ (\overline{2.15})^2\ (\overline{3.50}^2 - \overline{1.40})^2}$$

$$= 23{,}000 \text{ psi}$$

1. Stresses

At o.d. of Ring A:

$$f_t = \frac{b^2 p}{c^2 - b^2} \left(1 + \frac{c^2}{r^2}\right) = \frac{\overline{2.15}^2 (23{,}000)}{\overline{3.50}^2 - \overline{2.15}^2} \left(1 + \frac{\overline{3.50}^2}{\overline{3.50}^2}\right)$$

$$= 14{,}000\ (2) = 28{,}000 \text{ psi}$$

At A-B Interface:

$$f_t = 14{,}000 \left(1 + \frac{\overline{3.50}^2}{\overline{3.00}^2}\right) = 33{,}050 \text{ psi}$$

At B-C Interface:

$$f_t = 14{,}000 \left(1 + \frac{\overline{3.50}^2}{\overline{2.15}^2}\right) = 51{,}100 \text{ psi}$$

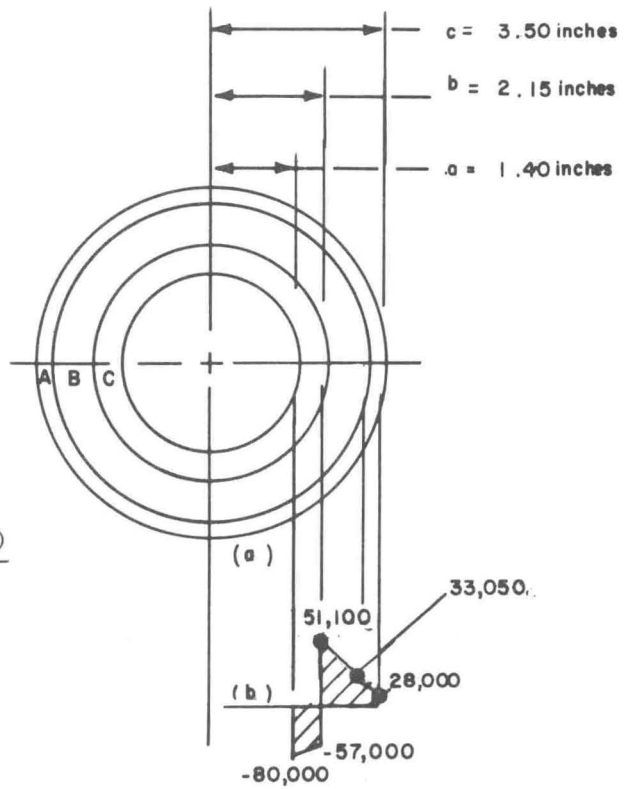

86-11265

Figure A-1 STRESS DISTRIBUTION DURING INSTALLATION OF RING C INTO A AND B

$$f_c = \frac{b^2 p}{(b^2 - a^2)} \left(1 + \frac{a^2}{r^2}\right) = \frac{2.15^2\,(23{,}000)}{(2.15^2 - 1.40^2)} \left(1 + \frac{1.40^2}{2.15^2}\right)$$

$$= 57{,}000 \text{ psi}$$

At i. d. of Ring C:

$$f_c = 40{,}000 \left(1 + \frac{1.40^2}{1.40^2}\right)$$

$$= 80{,}000 \text{ psi}$$

These stresses are plotted as shown in Figure A-1(b).

2. Strain Gage Data

From Table A-I an average reading of 30, 300 psi was recorded. (Readings indicate that strain gage No. 4 yielded higher values than the other three gages and showed up especially when Ring D was installed. Therefore, it was not included in the average value.) A 7.6 percent difference existed between the calculated (28, 000 psi) and test (30, 300 psi) values. It was concluded that these values are close enough for our intents and purposes.

3. Radial Displacement of i. d. Of Ring C Due To Ring C Installation (Figure A-2

$$\delta = \frac{2\,(b^2 p)(a)}{E\,(b^2 - a^2)} = \frac{2}{29 \times 10^6} \quad \frac{(2.15^2 \times 23{,}000)\,(1.40)}{(2.15^2 - 1.40^2)}$$

$$= 0.0038 \text{ inch}$$

This deflection is added to the existing interference (before assembly) of Ring D.

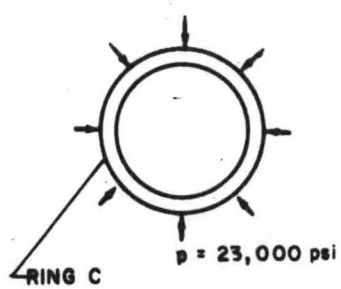

86-11266

Figure A-2 RADIAL DISPLACEMENT OF i.d. OF RING C DUE TO RING C INSTALLATION

TABLE A-1

RECORDED STRAIN AND STRESSES

Die	Gage No. 1		Gage No. 2		Gage No. 3		Gage No. 4	
Load (tons)	Strain (μin/in)	Stress (psi)	Strain (μin/in)	Stress (psi)	Strain (μin/in)	Stress (psi)	Strain (μin/in)	Stress (psi)
Ring C 36 Ring D 120	240 915	6, 960 26, 550	225 940	6, 530 27, 250	255 925	7, 400 26, 800	220 905	6, 380 26, 250
Punch No. 1								
Ring C 70 Ring D 130	1, 050 2, 520	30, 500 73, 000	1, 050 2, 520	30, 600 73, 000	1, 025 2, 480	29, 700 71, 900	1, 075 2, 640	31, 200 76, 500
Punch No. 2								
Ring B 0+ Ring C 65 Ring D 135	70 1, 125 2, 640	2, 030 32, 625 76, 560	60 1, 130 2, 605	1, 740 32, 770 75, 545	65 1, 090 2, 585	1, 885 31, 610 74, 965	65 1, 100 2, 630	1, 885 31, 900 76, 270

FINAL ASSEMBLY OF VEGA AND CENTERPIECE

Die								
60	210	6090				180	5220	
Punch No. 1								
79	280	8120				280	8120	
Punch No. 2								
70	340	9860	340	9860	320	9280	280	8120

B. INSTALLATION OF RING D INTO A, B, AND C (Figure A-3(a))

Total interference between Ring D and combination rings A, B, C is equal to existing interference (Table A-II) before assembly plus deflection due to radial displacement of i.d. of ring C during its installation into combination rings A, B. (Figure A-2)

δ total = 0.011 + 0.0038 = 0.0148 inch

Therefore

$$p = \frac{E\,\delta\,(b^2-a^2)\,(c^2-b^2)}{b(2b^2)\,(c^2-a^2)} \qquad (a)$$

$$= \frac{29\times10^6(0.0148)\,(\overline{1.41}^2-\overline{0.66}^2)(\overline{3.50}^2-\overline{1.41}^2)}{1.41\times2\times\overline{1.41}^2\,(\overline{3.50}^2-\overline{0.66}^2)}$$

= 103,000 psi

1. Stresses

At o.d. of Ring A:

$$f_c = \frac{b^2 p}{c^2-b^2}\left(1+\frac{c^2}{r^2}\right) = \frac{1.41^2(103{,}000)}{3.50^2-1.41^2}$$

$$\left(1+\frac{\overline{3.50}^2}{\overline{3.50}^2}\right) = 19800\,(2) = 39{,}600 \text{ psi}$$

At A-B Interface:

$$f_t = 19{,}800\left(1+\frac{\overline{3.50}^2}{\overline{3.0}^2}\right) = 47{,}000 \text{ psi}$$

At B-C Interface:

$$f_t = 19{,}800\left(1+\frac{\overline{3.50}^2}{\overline{2.15}^2}\right) = 72{,}700 \text{ psi}$$

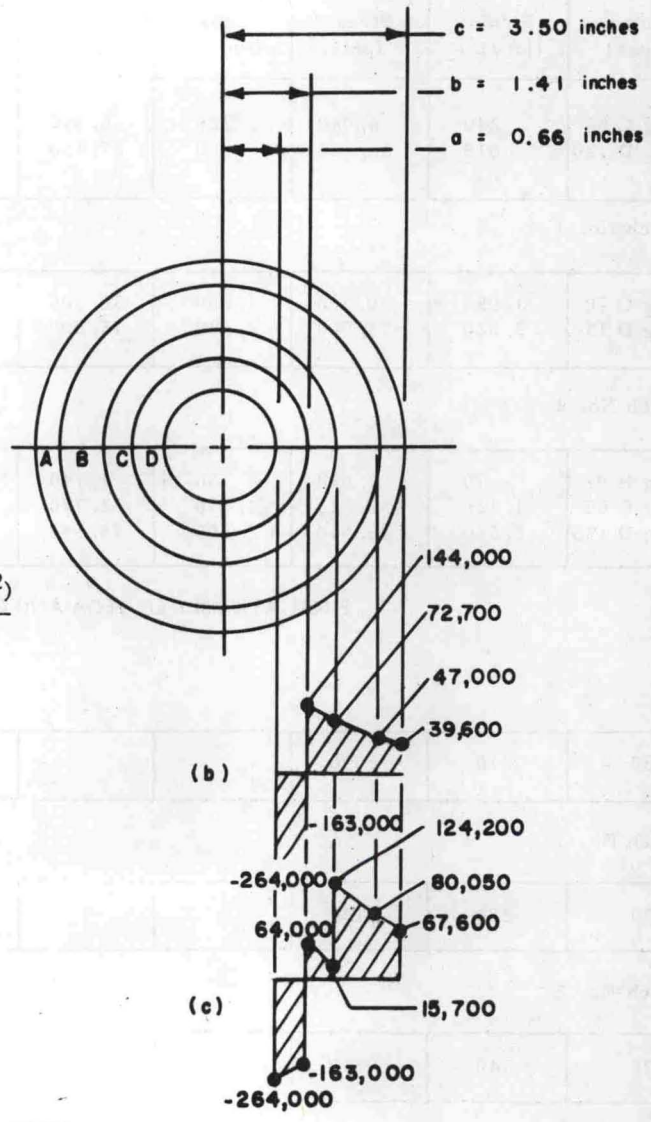

Figure A-3 STRESS DISTRIBUTION DURING INSTALLATION OF RING D INTO A, B AND C

TABLE A-II

FINAL DIMENSIONS BEFORE ASSEMBLY

	Die Ring A	Ring B Max	Ring B Min	Ring C Max	Ring C Min	Ring D Max	Ring D Min	Ring D After Assy.	Vega o.d.
o.d.	12.505	11.5005		7.498	7.378	5.500*	5.380*		No. 1 3.5005*
i.d.	11.500	7.483	7.363	5.478	5.358	3.500	3.380	3.365*	No. 2 3.5010*
									No. 3 3.5020*
	Punch No. 1								
o.d.	7.005	6.005		4.375	4.255	2.875	2.755*		1.375*
i.d.	6.000	4.359	4.239	2.853	2.733	1.375	1.350	1.325*	
	Punch No. 2								
o.d.	6.9995	6.0002		4.3752	4.2552	2.8752*	2.7552		
i.d.	6.0001	4.359	4.239	2.8533	2.7335	1.354	1.340		

The measurements of the die and punch No. 1 are all within 0.0005-inch. Those of punch No. 2 are as listed.

Final o.d. of Die A-Ring after assembly = 12.517 inches.
Final o.d. of Punch No. 1 A-Ring after assembly = 7.020 inches.
Final o.d. of Punch No. 2 A-Ring after assembly = 7.020 inches.

*These dimensions were not final before final assembly.

At C-D Interface: $f_t = 19,800 \left(1 + \frac{\overline{3.50}^2}{\overline{1.41}^2}\right) = 144,000$ psi

$$f_c = \frac{b^2 p}{b^2 - a^2}\left(1 + \frac{a^2}{r^2}\right) = \frac{\overline{1.41}^2 (103,000)}{\overline{1.41}^2 - \overline{0.66}^2}\left(1 + \frac{0.66^2}{1.41^2}\right)$$

$= 163,000$ psi

At i.d. of Ring D:

$$f_c = 132,000\left(1 + \frac{\overline{0.66}^2}{\overline{0.66}^2}\right) = 264,000 \text{ psi}$$

These stresses are plotted as shown in Figure A-3(b) and added to Figure A-1(b) values, the summation being shown as Figure A-3(c).

2. Strain Gage Data

From Table A-I an average reading of 72,600 psi was recorded. (Gage No. 4 was not averaged in for reasons outlined in Subsection A, 2). A 6.9-percent difference exists between the calculated (67,600 psi) and test (72,600 psi) values. These values agree close enough for our intents and purposes.

C. INSTALLATION OF CENTER ASSEMBLY INTO A, B, C, AND D. (Figure A-4)

The i.d. of Ring D was machined so that a 0.006-inch radial interference exists between the center assembly and combination rings A, B, C, and D.

It was assumed that no appreciable stresses were induced by the punch on the Vega since no interference or taper were built into its design.

For $\delta = 0.006$ inch

$$p = \frac{E\,\delta}{2bc^2}(c^2 - b^2) = \frac{29 \times 10^6 (0.006)(\overline{3.50}^2 - \overline{0.658}^2)}{2 \times 0.658 \times 3.50^2}$$

$= 128,000$ psi

1. Stresses

At o. d. of Ring A:

$$f_t = \frac{b^2 p}{c^2 - b^2}\left(1 + \frac{c^2}{r^2}\right)$$

$$= \frac{0.658^2\,(128{,}000)}{(\overline{3.50}^2 - \overline{0.658}^2)}\left(1 + \frac{\overline{3.50}^2}{\overline{3.50}^2}\right)$$

$$= 9340 \text{ psi}$$

At A-B Interface: f_t = 11,000 psi

At B-C Interface: f_t = 17,050 psi

At C-D Interface: f_t = 34,000 psi

At D-Center Assembly Interface:

f_t = 137,000 psi

$$f_c = \frac{p\,b^2}{b^2 - a^2}\left(1 + \frac{a^2}{r^2}\right)$$

$$= 128{,}000 \text{ psi}$$

At Center of Assembly:

$f_c = 2p = 256{,}000$ psi

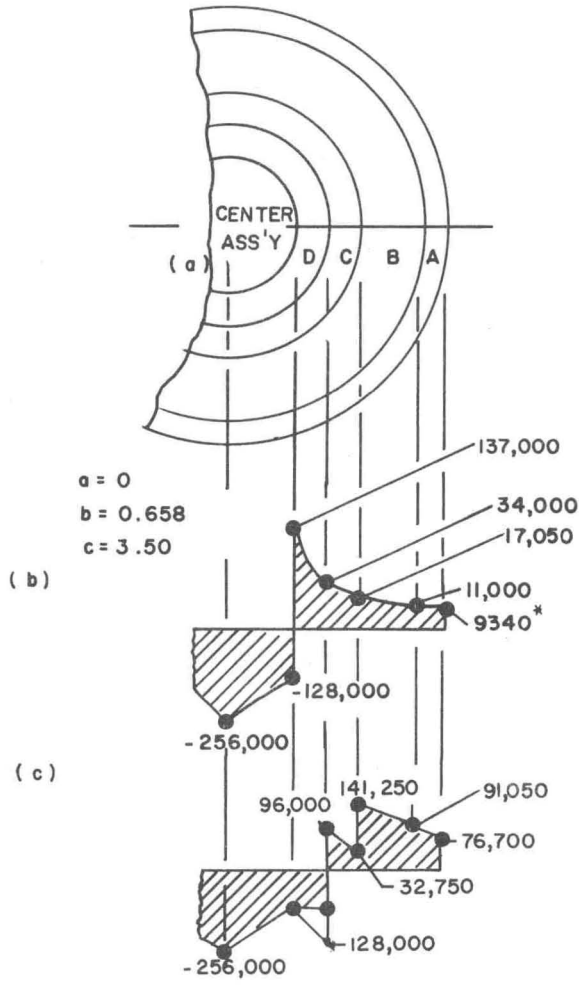

86-11268

Figure A–4 STRESSES ENCOUNTERED DURING INSTALLATION OF CENTER ASSEMBLY INTO A, B, C AND D

*From the test data, there was a scatter of this value varying from 8120 to 9860 psi. Therefore, based on this test data, it is reasonable to assume that the calculated value closely approximates the test data.

Assuming Poisson's Ratio of 0.30 and a downward developed pressure of 1 x 10^6 psi, the internal radial pressure is calculated by p = 0.30 (1,000,000) = 300,000 psi. This yields Figure A-5 (a) which is $\frac{300}{128}$ times Figure A-4 (b).

The final stress distribution is shown by Figure A-5 (b). The effect of the taper is negligible as compared to stresses caused by the interference fits.

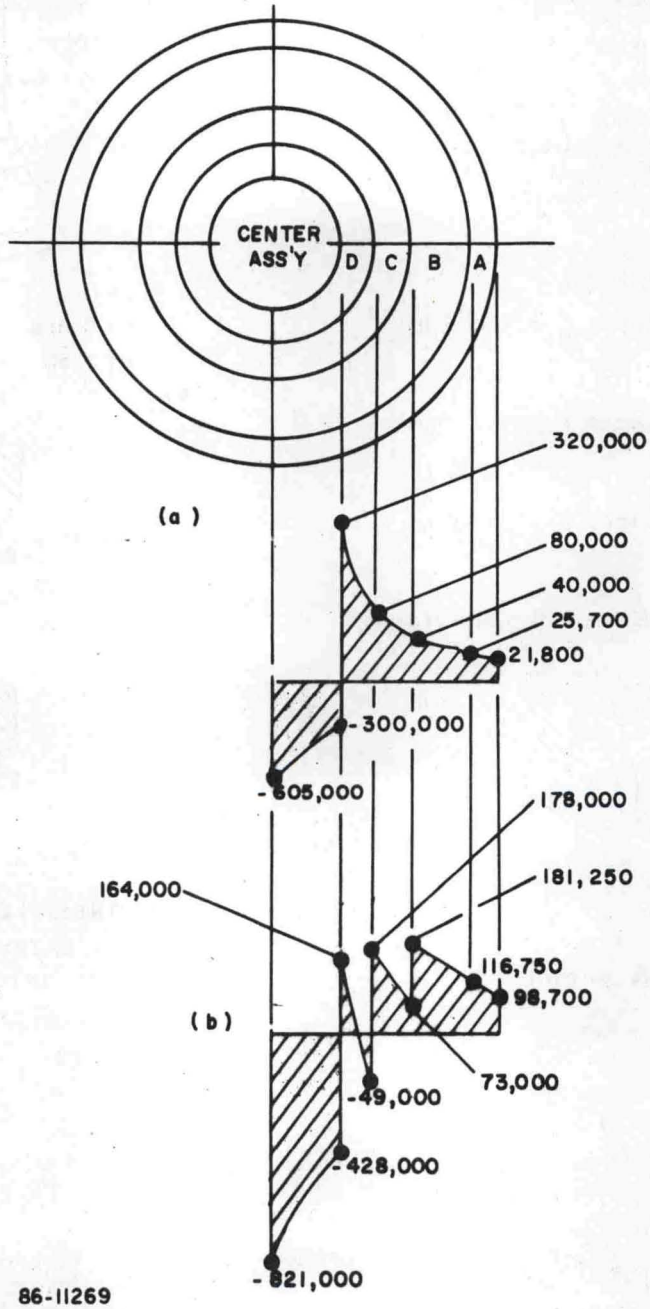

Figure A-5 (a) STRESS DISTRIBUTION DUE TO 300,000 psi INTERNAL RADIAL PRESSURE; (b) FINAL STRESS DISTRIBUTION

DIE ASSEMBLY

The correlation between test data and calculated values did not agree as well as that of the punch assembly. Because of this, two final stress distributions are presented, the first being that calculated from given interferences using the same formula and procedures as outlined for the punch assembly (Subsection A and B) and the second, using strain gage data presented in Table A-II and calculating final stress distributions by extrapolating computed values with test values.

From a study of Reference 14 it is not difficult to reason that a slight variation of the interference fit adversely affects our load parameters while slight geometry changes have negligible effects on the final stresses. It is not unreasonable to assume, therefore, that the given interference is slightly lower than recorded. However the overall effect on the magnitude of stresses of the two curves is not critical. This is shown on Figure A-6 (c) and (d).

Presented below are plots of stresses using Reference 14 and extrapolated strain gage data. (See Figures A-6 and A-7.)

ASSEMBLY

It is recommended that the outside surface of the die and punch be strain-gage tested and recordings taken during the use of the punch and die. There are two reasons for this request.

1. Comparison of the strain gage readings with the predicted stress values will provide an estimate of the magnitude of stresses throughout the punch and die assemblies and an impending failure could be predicted.

2. From the total load applied and the stresses recorded, and estimation of Poisson's ratio of the oxide can be computed.

Starting with zero stress reading (at room temperature) on the outside circumferential strain gages, the limiting stresses, during use of the punch and die, should be 2,270 psi for the die and 20,000 psi for the punch.

A summary diagram of the complete assembly together with the material property requirements is shown in Figure A-8. Figure A-9 shows the location of the strain gages applied during assembly and the location of minor scratches observed at that time. Figure A-10 through A-12 show 1) the axial displacement of the rings, prior to assembly, due to the interference required for preloading, and 2) press loads required for assembly.

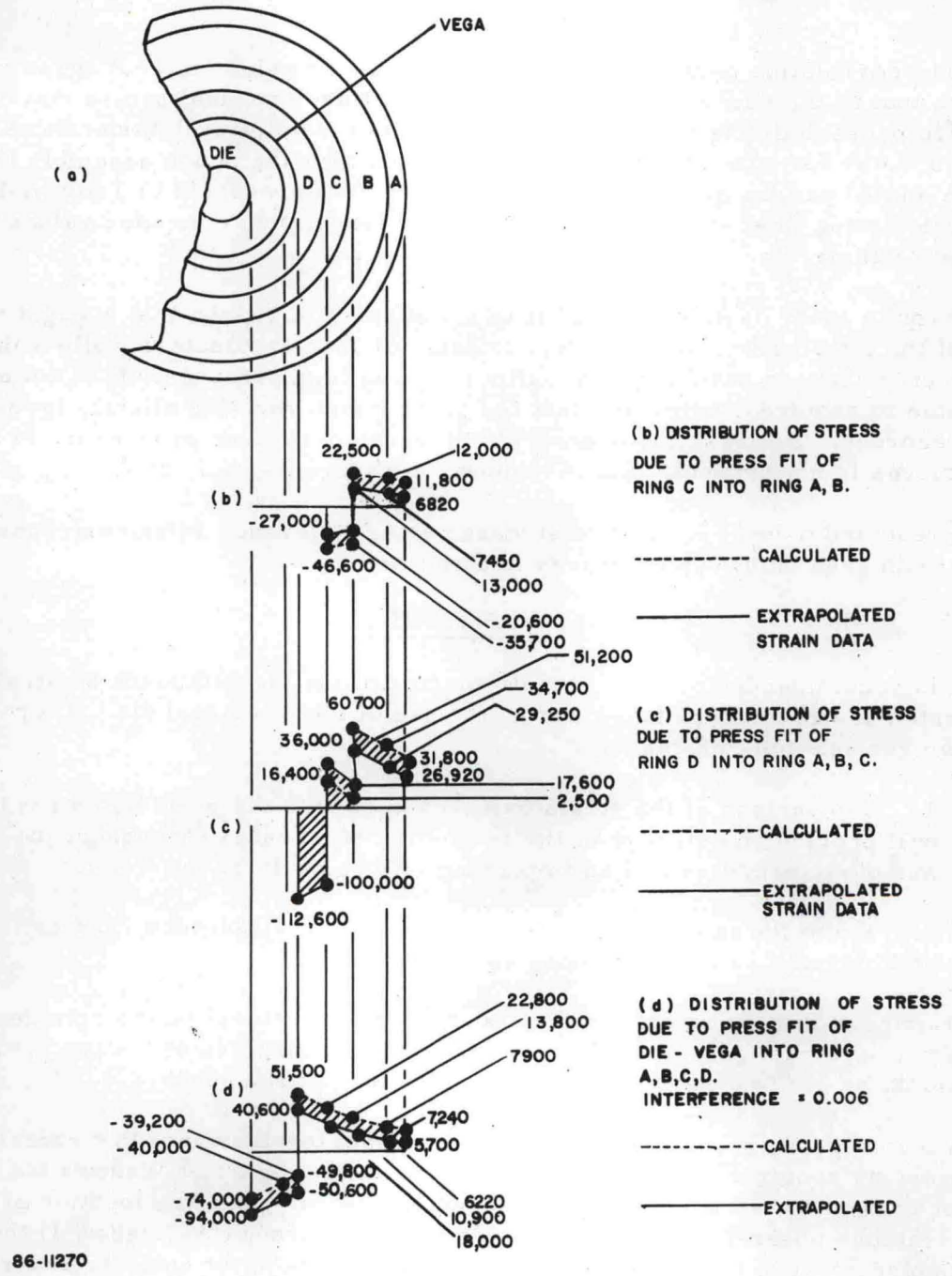

Figure A-6 FINAL STRESS ANALYSIS OF DIE ASSEMBLY

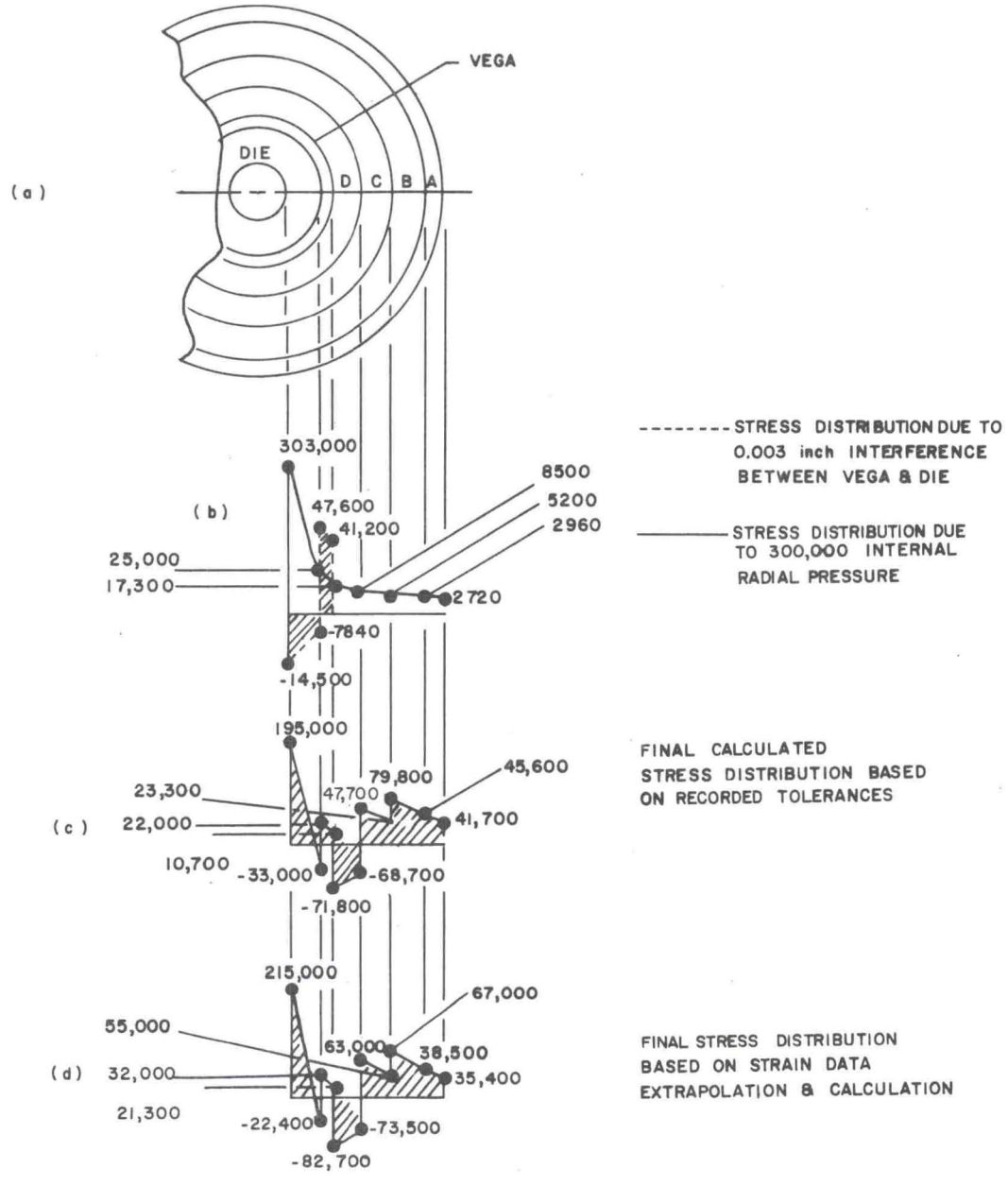

86-11271

Figure A-7 FINAL STRESS ANALYSIS OF DIE ASSEMBLY WITH 300,000 psi INTERNAL RADIAL PRESSURE

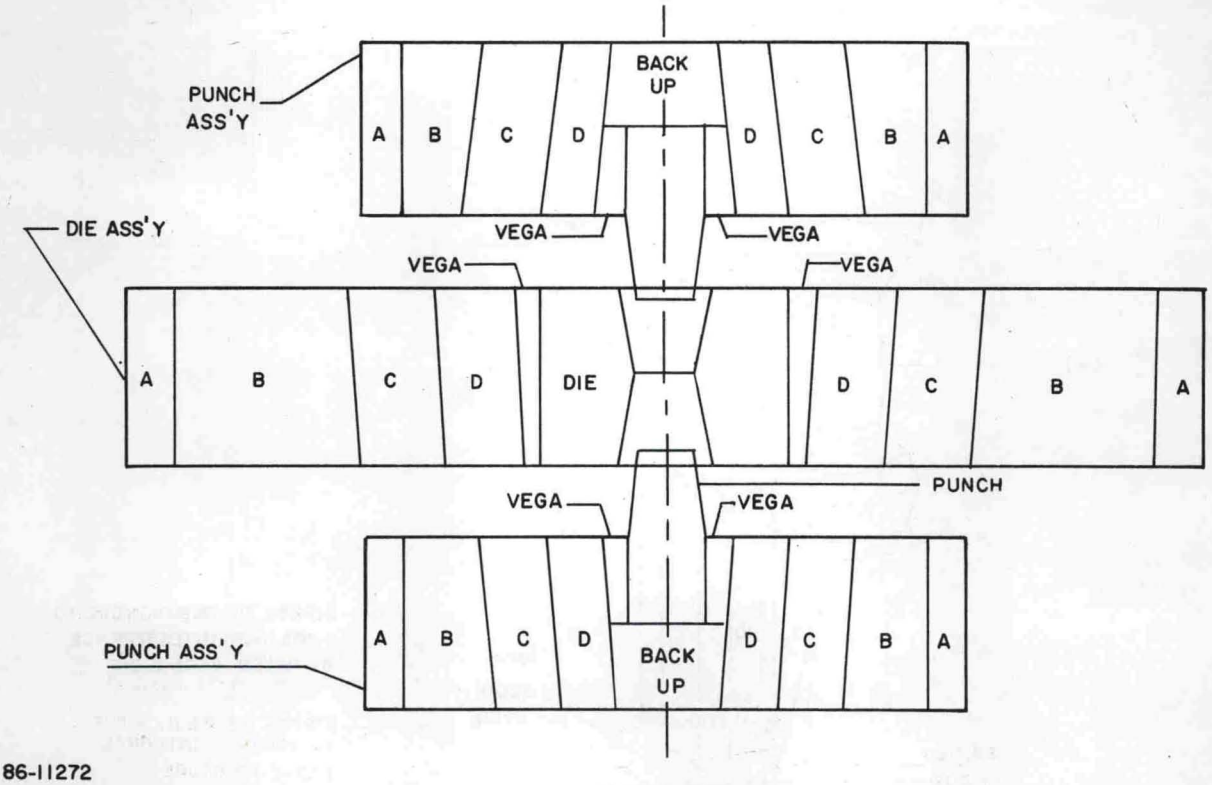

Figure A–8 SCHEMATIC OF HIGH-PRESSURE APPARATUS AND RELATIVE HARDNESS OF RINGS

Punch Assembly

Ring A: 4340 steel, RC 32-36
Ring B: 4340 steel, RC 40-45
Ring C: 4340 steel, RC 48-52
Ring D: 4340 steel, RC 48-52
Back Up: At least as hard as punch, RC 60-61
Vega: Vega steel, RC 55-58
Punch: 0.7500" Diameter with 5 degree taper, nondeforming steel Containing 0.90 to 1.10 percent Carbon, 5 percent Cr, RC 58-60.

Die Assembly

Ring A: 4340 steel, RC 32-36
Ring B: 4340 steel, RC 40-45
Ring C: 4340 steel, RC 48-52
Ring D: 4340 steel, RC 48-52
Vega: Vega steel, RC 55-58
Die: 0.7500" i.d. with 5 degree taper, nondeforming steel containing 0.90 to 1.10 percent Carbon, 5 percent Cr, RC 58-60.

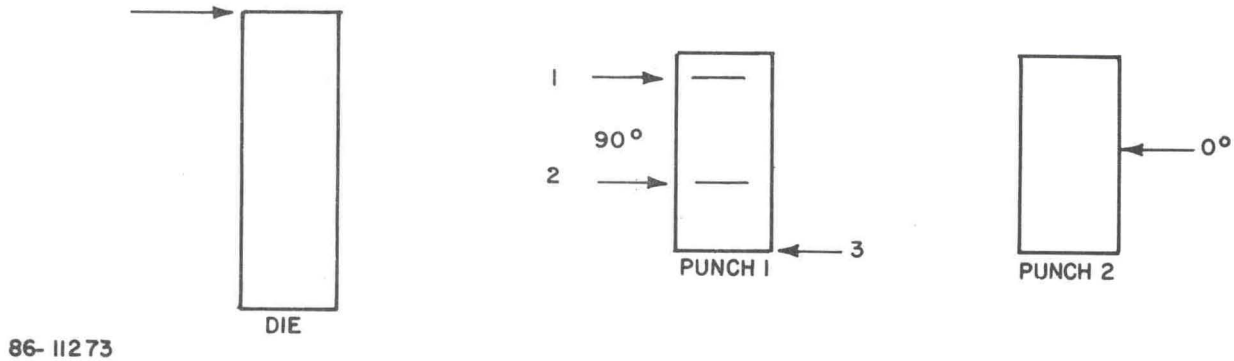

Figure A-9 VISUALLY OBSERVED RING IMPERFECTIONS

Die Outer Ring (A)

At 0 degrees the deep notch is approximately 3/32 of an inch wide by 1/8 of an inch long by 1/64 of an inch deep. The other two notches are small and not deep enough to measure.

All three were stoned and the edges smoothed out before assembly.

No. 1 strain gage was mounted at the 0-degree point. No. 2, 3, 4 gages were placed at 90, 180, 270 degrees respectively in a clockwise direction looking in the top.

Ring B was mounted into Ring A before the strain gages were installed on the latter.

Punch No. 1 Outer Ring (A)

This ring has two fine lines as shown by arrows 1 and 2. These lines, as well as the spot No. 3, are not scratches or notches made after machining. They appear to have been there before machining. However No. 1 is a fine line 5/16 inch long, No. 2 is 1/32 inch wide and 7/32 inch long, and No. 3 is 1/32 inch wide by 3/8 inch long.

Punch No. 2 Outer Ring (A)

The outer ring has a notch at approximately 45 degrees from its axis. The notch measures 7/16 inch long, 1/4 inch wide, and no more than 0.003 inch deep. A strain gage was mounted at 0 degrees near the notch and three others at 90, 180, and 270 degrees from the first one.

All other rings were visually inspected and no apparent nicks or notches were detected.

All strain gages were mounted 1 inch from either edge to read circumferential tensile stresses.

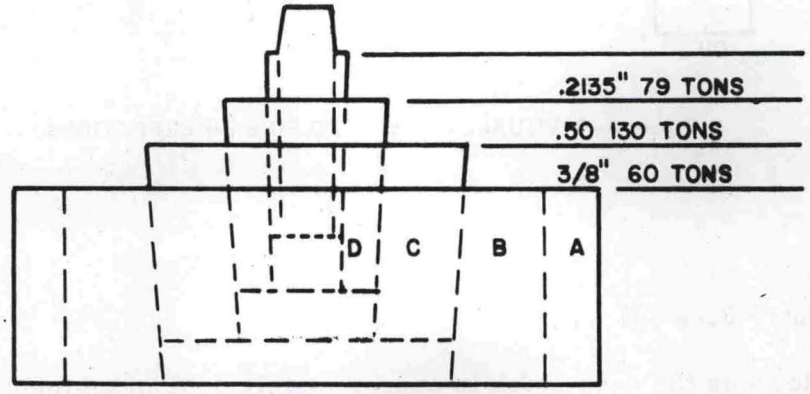

86-11274

Figure A–10 PUNCH ASSEMBLY NUMBER 1

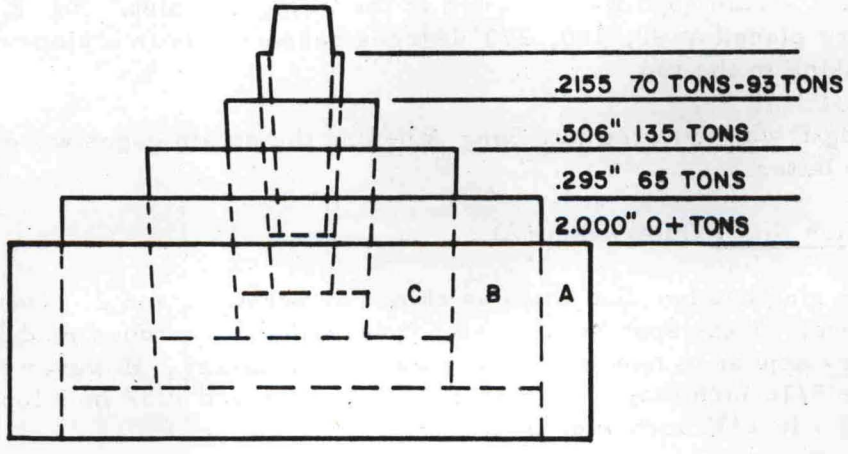

86-11275

Figure A–11 PUNCH ASSEMBLY NUMBER 2

Note: The above diagrams show (schematically) the interference between each of the Punch elements, and the corresponding force required to assemble each element.

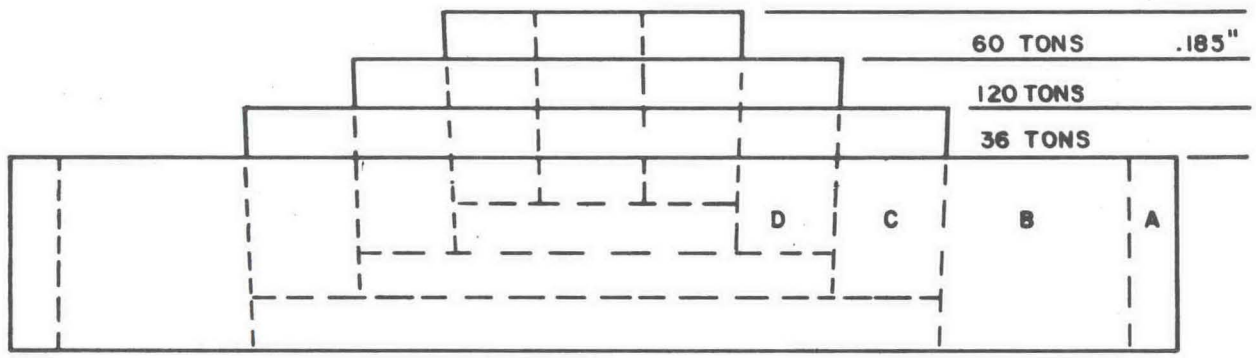

86-11276

Figure A–12 DIE ASSEMBLY INTERFACE DIAGRAM

Note: The above shows (schematically) the interference between each of the Die elements, and the corresponding force required to assemble each element.

APPENDIX B

COMPRESSIBILITY MEASUREMENTS PERFORMED WITH THE HIGH-PRESSURE CAMERA

APPENDIX B

	Sample	Radiation	Nominal Pressure (kilobars)	Time (hours)	Results and Comments
1	Checked out	Ag	0	8	Blank test run, no diamonds
2	Checked out	Ag	0	8	Blank test run, no diamonds
3	Checked out	Ag	0	8	Blank test run, no diamonds
4	Checked out	Ag	0	20	Blank test run, no diamonds
5	Bi	Ag	0	20	Blank test run, punch only
6	Bi	Ag	0		
7	Al	Ag	0		
8	Al	Ag	0		4 Al lines
9	Al	Ag	15 0	20 20	5 Al lines, no splitting observed
10	Al	Ag	15		
11	Al	Cu			No rings diamonds found out of mount
12	Al	Cu			Punch diamond found loose
13	KNO_3	Ag	0	20	1 half-line
14	KNO_3	Ag	5		Sample extruded
15	KNO_3	Ag	5		Insert way out of line Started using "fixed" piston
16	KNO_3	Ag	0.5		
17		Ag	5		Diamond found broken
18	None	Ag			
19	KNO_3 in Duco	Ag			6 lines very faint
20	KNO_3 in Duco	Ag/Rh			Rhodium lines from filter near sample
21	KNO_3 in Duco	Cu/Ni	0	20	Lower background but poor penetration by Cu radiation
22	KNO_3 in Duco	Cu/Ni	0	40	
23	KNO_3 in Duco	Cu/Ni	0	7	Lower background but poor penetration by Cu radiation

APPENDIX B (Cont'd)

	Sample	Radiation	Nominal Pressure (kilobars)	Time (hours)	Results and Comments
24	KNO_3	Cu/Ni	0	20	Lower background but poor penetration by Cu radiation
25	KI-Duco	Ag/Rh	0	20	
26	KI-Duco	Ag			
27	KI-Parlodion	Ag/Rh	0		
28	KI-Parlodion	Ag	0		
29	KI-Parlodion	Ag/Rh	0		
30	KI-Parlodion	Ag/Rh	5 0	40 20	
31	KI-Parlodion	Ag/Rh	0	20	
32	KI-Parlodion		0 5	20 40	
33	KI-Parlodion		0 10	40 40	
34	KI-Parlodion		0 10	40 40	
35	KI		0	40	6 splits KI
36	KI + NaCl		0	40	
37	KI + NaCl + Cu grid		0 10	40 40	First grid mount
38	KI + NaCl + Cu grid		0 10	40 40	
39	KI + NaCl + Cu		0 10	40 66	
40	RbCl + NaCl + Cu		0	40	
41	RbCl-NaCl	Ag/Rh	10 0	68 40	
42					
43	RbCl-NaCl	Ag/Rh	10	40	
44	RbCl-NaCl	Ag/Rh	10 0	80 63	
45	RbCl-NaCl	Ag/Rh	10	40	

	Sample	Radiation	Nominal Pressure (kilobars)	Time (hours)	Results and Comments
46					
47	RbCl-NaCl	Ag/Rh	5 0	48 48	
48	KCI NaCl	Ag/Rh	10 0	40 40	No observable splitting
49	KCI NaCl	Ag/Rh	5 0	48 40	1 line of KCI-II
50	KCI NaCl	Ag/Rh	10	40	No KCI-II
51	KCI NaCl	Ag/Rh	10 10	20 51	Alignment check
52	KCI NaCl	Ag/Rh	0 10	71 52	Good line splitting, see text
53	KCI NaCl	Ag/Rh	0 15	88 45	Good line splitting, see text
54	KCI NaCl	Ag/Rh	0 15	46 65	Good line splitting, see text
55	KCI NaCl	Ag/Rh	0	65	Good line splitting, see text
56	MgO	Ag/Rh	10 10	22 40	Alignment check No observable split
57	MgO	Ag/Rh	0 15	40 40	
58	MgO	Ag/Rh	0	40	1 split = 0.1277
59	MgO + RbCl	Ag/Rh	0 15	20 40	Alignment check
60	MgO + RbCl	Ag/Rh	10	40	Good line splitting, RbCl-II
61	RbCl + MgO	Ag/Rh	0 6	40 40	See text
62	RbCl + MgO	Ag/Rh	0	40	See text
63	RbCl + MgO	Ag/Rh	10 10	20 20	See text
64	RbCl + MgO	Ag/Rh	0	20	See text
65	BN (cubic) Cu grids	Ag	0	17	7 lines Hex BN shown
66	BN (cubic) Cu grids	Ag/Rh	0 10	24 22	Cu interference with cubic BN

APPENDIX B (Cont'd)

	Sample	Radiation	Nominal Pressure (kilobars)	Time (hours)	Results and Comments
67	BN (cubic) Cu grids	Ag/Rh	0 15	45 40	
68	BN (cubic) Cu grids	Ag/Rh	0 15	20 46	
69	Al grids	Ag/Rh	0 15	41 46	
70	Al grids	Mo/Zr	0	46	
71	Al grids	Mo/Zr	15 0	44 44	
72	Al grids	Mo/Zr	0	90	
73	RbCl	Ag/Rh	5	15	New diamond, check run
74	BN NaCl Cu grids	Ag/Rh	0	20	NaCl lines only
75	Cu grids	Ag/Rh	10	20	Diamonds broken
76	Cu grids	Ag/Rh	0.5	44	NaCl lines
77	Cu grids	Ag/Rh	5	42	An interference
78	Cu grids	Mo/Zr	5 5	40 48	
79	Cu grids	Mo/Zr	0	48	
80	Cu grids	Mo/Zr	2.5	17	Good NaCl, spotty BN
81	BN - NaCl	Mo/Zr	5 0 0	24 24 40	Good NaCl, spotty BN no splitting
82	RbBr RbCl	Mo/Zr	5	40	RbCl-I, RbCl-II, RbBr Observed
83	RbBr RbCl	Mo/Zr	0 4	40 52	Low intensity
84	RbBr RbCl	Mo/Zr	0 4	52 44	Cu retaining ring extruded over X-ray beam
85	RbBr RbCl	Mo/Zr	0	45	
86	RbBr	Mo/Zr	0	43	Very weak, sample extruded
87	RbBr	Mo/Zr	5 5	26 25	Single phase RbBr-II

	Sample	Radiation	Nominal Pressure (kilobars)	Time (hours)	Results and Comments
88	RbBr	Mo/Zr	0 4	21 46	Two phases equally intense, RbBr-I strong
89	RbBr	Mo/Zr	0 3	44 47	RbBr-II weak
90	RbBr	Mo/Zr	0	44	RbBr-II weak
91	RbBr	Mo/Zr	9 5	44 45	RbBr-II weak
92	RbBr	Mo/Zr	5	20	Single phase RbBr-I
93	RbBr	Mo/Zr	0	20	Single phase RbBr-I
94	RbBr	Mo/Zr	5 8	22 24	Two phase, RbBr-I weak
95	RbBr	Mo/Zr	5	24	RbBr-II strong
96	RbBr	Mo/Zr	4	23	Two phase
97	RbBr	Mo/Zr	3.5	24	Two phase
98	RbBr	Mo/Zr	3	23	Two phase
99	RbBr	Mo/Zr	5	22	Two phase
100	RbBr	Mo/Zr	5 0	40 30	Two phase, no splitting
101	RbBr	Mo/Zr	0 0	63 30	Single phase RbBr-I
102	RbBr	Mo/Zr	5 0	41 32	Two phase; both apparently split
103	RbBr	Mo/Zr	5 10	41 26	Two phase, RbBr-II split
104	RbBr	Mo/Zr	5 10	23 27.5	Two phase, RbBr-II split
105	RbBr	Mo/Zr	5 8	26 25	Single phase, RbBr-II split
106	RbBr	Mo/Zr	5 10	28 23	Single phase, RbBr-II split

	Sample	Radiation	Nominal Pressure (kilobars)	Time (hours)	Results and Comments
107	RbBr	Mo/Zr	5 8	24 24	Single phase, RbBr-II split
108	RbBr	Mo/Zr	5	23	Single phase, RbBr-II split
109	RbBr	Mo/Zr	5	28	Single phase, RbBr-II split
110	RbBr	Mo/Zr	10	24	Single phase, RbBr-II split
111	RbBr	Mo/Zr	0	24	Single phase, RbBr-I only
112	RbBr	Mo/Zr	0.8	12	First with Parson diamond in inserted mount, see text
113	RbBr	Mo/Zr	1.3	27	Two phase
114	RbBr	Mo/Zr	1.3	24	Two phase
115	RbBr + NaCl	Mo/Zr	0.4 0.4	24 24	RbBr; NaCl interferes with RbBr-II
116	RbBr + NaCl	Mo/Zr	0	24	RbBr; NaCl interferes with RbBr-II
117	RbBr + NaCl	Mo/Zr	1.45	24	RbBr; NaCl interferes with RbBr-II
118	RbBr + NaCl	Mo/Zr	0 1	24 24	RbBr; NaCl interferes with RbBr-II
119	RbBr + NaCl	Mo/Zr	0	24	RbBr; NaCl interferes with RbBr-II
120	RbBr + NaI	Mo/Zr	1	24	Single phase = 7.23, see text
121	RbBr + NaI	Mo/Zr	1.5	24	Single phase = 7.23, see text
122	RbBr + NaI	Mo/Zr	1	21	Single phase = 7.23, see text
123	RbBr + Ag	Mo/Zr	1 1.5	44 22	RbBr-I, RbBr-II + Ag
124	RbBr + Ag	Mo/Zr	1.0	23	Ag interferences with both RbBr
125	RbBr + Ag	Mo/Zr	1.5	22	
126	RbBr + Ag	Mo/Zr	2 2	22 23	
127	RbBr + Ag	Mo/Zr	1 1	23 23	
128	RbBr + NaCl + Ag	Mo/Zr	0 2	23 23	

APPENDIX B (Concl'd)

	Sample	Radiation	Nominal Pressure (kilobars)	Time (hours)	Results and Comments
129	RbBr + NaCl + Ag	Mo/Zr	0	22	
130	NaCl + Ag	Mo/Zr	3	22	
			0	22	
131	NaCl + Ag	Mo/Zr	3	21	
132	NaCl + Ag	Mo/Zr	0	23	
133	RbBr + Pt	Mo/Zr	2	23	Parson diamond in standard mount
134	RbBr + Pt	Mo/Zr	5	23	
			5	22	
135	RbBr + Pt	Mo/Zr	0	22	
136	RbBr + Pt	Mo/Zr	4	23	
			4	23	
137	RbBr + Pt	Mo/Zr	2	23	
			2	23	
138	RbBr + Pt	Mo/Zr	1	23	
			1	23	
139	RbBr + Pt	Mo/Zr	0	23	
140	RbBr + Pt	Mo/Zr	0.5	23	After prepress at 5 kilobars
141	RbBr + Pt	Mo/Zr	0.7	23	
			0.7	23	
142	RbBr + Pt	Mo/Zr	0	23	
			5	23	
143	RbBr + Pt	Mo/Zr	1	23	

APPENDIX C

HIGH-PREPARE RUNS MADE WITH THE "BELT"-TYPE APPARATUS

Run No.	Temp. (°C)	Pressure (psi)	Time (min)	Results
9A	350*	250, 000	11	0. 092 micron, bluish color, small grain.
10A	150*	250, 000	10	Not dense, poor sample.
11A	280*	250, 000	12	Not dense, low power.
15A	790*	250, 000	13	Laminated, high density, bluish, 0. 379 micron.
20A	800*	250, 000	5	Laminated, dark blue sample, 0. 114 micron.
21A	620*	250, 000	10	Laminated, high density, slightly blue.
22A	720*	250, 000	8	Laminated, high density, almost black.
24A	1190	250, 000	3	Four pieces white except at ends (blue), 0. 314 micron.
25A	725*	250, 000	6	Dense, bluish, white.
26A	800*	250, 000	3	Disks, transparent and milky pieces.
30A	800*	250, 000	5	Disks, delaminated, transparent, translucent thick pieces.
31A	620*	250, 000	4	Delaminated, disks 1/16 inch approx. All disks translucent. Some were transparent.
32A	725*	250, 000	5	Two phases, present in MgO translucent and opaque.
1B	1060	23, 970	12	No delamination present--cracked during cutting.
2B	640	57, 900	8	Leak in vacuum. Sample collapsed, very porous.
3B	730	57, 900	8	Sample very porous.
4B	1220	15, 000	5	Circuit broke.
5B	1050	30, 000	5	Sample began to densify. Not held long enough at temperature.
6B	1180	31, 000	3	No results.
7B	1530	31, 000	4	Pieces of samples scratched Rc57 tool steel.
8B	796	45, 000	10	Sample didn't densify. Thermocouple shorted.
9B	350*	63, 000	2	Thermocouple shorted 63, 000 psi. Punch crack. Porous sample.
10B	1600	45, 000	9	1047KHN, density of sample was determined H_2O 93% dense, pore open.
11B	725*	72, 000	9	70KHN, MgO translucent. Some stuck to Ni. Dense 90% of 10.
12B	920	31, 000	2	1128 KHN MgO translucent. Top was opaque. It was fully dense.
13B	1100	31, 000	3	MgO pieces were obtained. Seemed dense. Not hard enough to scratch Rc57 steel.
14B	1015	31, 000	5	Sample very hard. Scratch Rc57, steel pieces were small.
15B	850*	31, 000	3	Sample looked denser. Pieces were grey, some white.
17B	1100	31, 000	5	Majority of samples dense. Quite porous.
18B	990*	70, 000	4	97%. Dense.
19B	875	75, 000	2	Pressed 50% of its length. Smoky quartz, scratch Rc57.
20B	1000*	75, 000	5	Large pieces MgO obtained were dense, translucent.
21B	1000	75, 000	4	Sample 45°. Sample dense--not as hard as others.
22B	900	60, 000	3	450KHN, two large pieces obtained. One sent to metallography to polish.

* Temperature estimated for power.

Run No.	Temp. (°C)	Pressure (psi)	Time (min)	Results
19C	910*	250, 000	5	Black specks of graphite. Very porous.
21C	870*	250, 000	10	Many delaminated transparent disks formed.
20C	920	250, 000	10	Many small pieces of transparent MgO.
24C	500*	250, 000	3	Temperature too low. Black MgO--unreacted MgO.
25C	900*	250, 000	5	Poor run, very porous, not prepressed.
31C	850*	500, 000	5	Black MgO obtained. Temperature too low.
33C	1000*	500, 000	6	Black material formed. Very porous, poor.
45C	845	250, 000	10	Given to AFCRL.
53C	850	250, 000	10	
54C	900	250, 000	10	
56C	910	250, 000	10	
57C	1020	250, 000	10	
58C	855	250, 000	10	
60C	948	110, 000	10	Bend specimen, modulus of rupture 26, 000 psi.
61C	1105	110, 000	10	
62C	950	110, 000	10	Modulus rupture 29, 600 psi and 8000 (crazed piece).
63C	800	110, 000	10	
68C	950	110, 000	45	
69C	930	110, 000	30	
70C	960	110, 000	32	
74C	1015*	110, 000	12	
75C	940	110, 000	30	
76C	935	110, 000	30	
77C	1100	110, 000	30	
78C	970	110, 000	30	
79C	940	110, 000	30	Modulus rupture 9670 psi (crazed piece).
80C	700	45, 000		Vacuum chamber short circuit, sample very porous.
82C	870	110, 000	10	Cracked, sent to AFCRL for IR spectra.
83C	800	110, 000	10	Submitted, AFCRL for IR spectra.
84C	990	110, 000	10	Cracked.
85C	1000	110, 000	10	Cracked.
86C	870	110, 000	10	Cracked.
87C	990	110, 000	13	Sent to AFCRL for IR Spectra.
88C	1105	110, 000		Sent to AFCRL for IR Spectra.
89C	1000*	110, 000	30	Cracked.
90C	980	110, 000	30	Cracked.

*Temperature estimated for power.

NiO

Run No.	Temp (°C)	Pressure (psi)	Grain Size (microns)	Time (min)	KHN	Results
11C	940	250, 000	0.55	8	764	Good sample, very brittle, delaminated.
14C	890 (1360)	250, 000		12	575	Good sample.
17C	910 (1271)	500, 000		10		Very poor.
18C	1000* (1656)	500, 000		2		Highly delaminated.
22C	1300* (1788)	250, 000	0.32	10	800	Two large pieces, did not delaminate.
23C	990 (1591)	250, 000	0.52	10	134	Delaminated 6 large pieces. Green on end, middle black.
27C	980* (1586)	250, 000	0.34	9	728	Delaminated, large disks.
32C	1000 (1664)	500, 000				Delaminated large porous disks (single crystals).
34C	960* (1439)	500, 000		10		Delaminated, porous.

*Temperature estimated from power in parenthesis.

Cr_2O_3

Run No.	Temp. (°C)	Pressure (psi)	Time (min)	Grain Size	Results
12C	1400	250, 000	10	0.85	116KHN, fair structure, fibrous structure
15C	940*	500, 000	10		Very poor, crumbled piece, dense in middle
16C	1580*	250, 000	3	0.22	1364KHN, poor disk sent to metallography.
28C	1260*	250, 000	4	0.38	Fair, too porous to test.
29C	1230*	250, 000	6	0.28	91KHN, delaminated, very porous.
30C	1350	500, 000	4		Very poor, reacted with heater.

* Temperature estimated for power.

Al_2O_3

Run No.	Temp. (°C)	Pressure (psi)	Grain Size (mm)	Hardness (KHN)	Time	(misc.)	Results
12A	NA	250, 000			10		Temperature too low, powder
13A	NA	250, 000			9		No densification
14A	NA	250, 000			14		No densification
16A	NA	250, 000			10		Slightly dense, no strength
17A	NA	250, 000			5		Dense, Al_2O_3 formed
1C	320	250, 000			10		Sample cut longwise, many cracks. Two distinct areas.
2C	NA	250, 000			3		High hardness, different grain sizes.
3C	NA	250, 000			7		Sample cut long, distinct areas (2).
4C	NA	250, 000			3		Sample broke in many pieces, opaque. Not hard.
6C	1380	250, 000			4		Disk obtained, large grain size and high temperature
7C	NA	250, 000	0.0005		10		Sample cut lengthwise.
8C	NA	250, 000	0.025	1600	3		Sample delaminated
9C	NA	45, 000		2000	10		Melted Ni sleeve 1453° C, punch oxidized. No samples.
10C	1500	250, 000	0.015	2000	4		Delaminated large disk.
98B	1000	31, 000			5		
100B	1050	45, 000			18		Al_2O_3 separated from Ni tube. Some spinel formed on periphery
102B	1300	31, 000			1		
105B	1055				7		

DISTRIBUTION

Addressee	No. of Copies
Hq., ARCRL, OAR (CRWA) STOP 30 L. G. Hanscom Field Bedford, Massachusetts 01730 CRL-C	1
AFCRL (CRMXLR) STOP 29 L. G. Hanscom Field Bedford, Massachusetts 01730 CRL-C	3
AFCRL (CRMXLR) STOP 29 Attn. Mrs. Cora Gibson L. G. Hanscom Field Bedford, Massachusetts 01730 CRL-C	2
AFCRL (CRMXRA) STOP 39 L. G. Hanscom Field Bedford, Massachusetts 01730 CRL-C	10
AFCRL (CRMXRD) STOP 30 L. G. Hanscom Field Bedford, Massachusetts 01730 CRL-C	1
AFCRL (CRN) STOP 30 L. G. Hanscom Field Bedford, Massachusetts 01730 CRL-C	1
AFCRL (CRTE) STOP 30 L. G. Hanscom Field Bedford, Massachusetts 01730 CRL-C	1
AFCRL (CRTPM) STOP 30 L. G. Hanscom Field Bedford, Massachusetts 01730 CRL-C	1

DISTRIBUTION (Cont'd)

Addressee	No. of Copies
ADC Operations Analysis Office Ent. Air Force Base Colorado 80912 CRL-C	1
AEDC (ARO, INC.) Attn. Library/Documents Arnold Air Force Station Tennessee 37389 CRL-C	1
AFETR Technical Library-MU-135 Patrick Air Force Base Florida 32925 CRL-C	1
AFIT (MCLI. LIBRARY) Building 640 Area B Wright-Patterson Air Force Base Ohio 45433 CRL-C	1
AFSC-STLO (RSTAL) AF Unit Post Office Los Angeles, California 90045 CRL-C	1
AFSG-STLO (RTSAB) Waltham Federal Center 424 Trapelo Road Waltham, Massachusetts 02154 CRL-C	1
AFSC-STLO (RTSUM) 68 Albany Street Cambridge, Massachusetts 02139 CRL-C	1

DISTRIBUTION (Cont'd)

Addressee	No. of Copies
AFWL (WLIL) Kirtland Air Force Base New Mexico 87117 CRL-C	1
Dir., Air University Library Attn. AUL3T Maxwell Air Force Base Alabama 36112 CRL-C	1
APGC (?GB?S-12) Eglin Air Force Base Florida 32542 CRL-C	1
Hq. AWSAE/SIPB Scott Air Force Base Illinois 62225 CRL-C	1
OAR (RRY) 1400 Wilson Boulevard Arlington, Virginia 22209 CRL-C	1
RADC (EMTLD) Attn. Documents Library Griffiss Air Force Base New York 13440 CRL-C	1
RTD Scientific Director Bolling Air Force Base Washington, D.C. CRL-C	1
RTD (AWX) Wright-Patterson Air Force Base Ohio 45433 CRL-C	1

DISTRIBUTION (Cont'd)

Addressee	No. of Copies
SAC (OAI) Offutt Air Force Base Nebraska 68113 CRL-C	1
Systems Engineering Group (RTD) Attn. SEPIR Wright-Patterson Air Force Base Ohio 45433 CRL-C	1
SSD (SSTRT) Attn. Lt. O'Brien Los Angeles Air Force Station AFUPO Los Angeles, California 90045 CRL-C	1
Hq., TAC (OA) Langley Air Force Base Virginia 23362 CRL-C	1
USAF Academy Academy Library (DFSLB) Colorado 80840 CRL-C	1
USAF Academy FJSRL Colorado 80840 CRL-C	1
Hq., USAFSS (OSA) San Antonio Texas 78241 CRL-C	1
Army Electronic Proving Ground Technical Library Fort Huachuca, Arizona CRL-C	1

DISTRIBUTION (Cont'd)

Addressee	No. of Copies
Army Missile Command Attn. Chief, Document Section Redstone Scientific Info. Center Redstone Arsenal, Alabama 35809 CRL-C	1
Los Alamos Scientific Laboratory Post Office Box 1663 Los Alamos New Mexico 87544 CRL-C	1
U.S. Army Electronics Command Attn: AMSEL-RD-MAT Technical Document Center Fort Monmouth, New Jersey 07703 CRL-C	1
U.S. Army Research Office Attn. Technical Library 3045 Columbia Pike Arlington, Virginia 22204 CRL-C	1
Bureau of Naval Weapons (DLI-31-Library) Washington, D.C. CRL-C	1
Chief of Naval Operations (OP-413-B21) Washington, D.C. CRL-C	1
Naval Air Development Center Library Johnsville, Pennsylvania CRL-C	1
Naval Missile Center Library Point Mugu, California CRL-C	1

DISTRIBUTION (Cont'd)

Addressee	No. of Copies
Naval Ordnance Laboratory Technical Library White Oak, Silver Spring Maryland 20910 CRL-C	1
Director Naval Research Laboratory Attn. 2027 Washington, D.C. 20390 CRL-C	1
Commander (Code 753) U.S. Naval Ordnance Test Station Attn. Technical Library China Lake, California 93555 CRL-C	1
U.S. Naval Postgraduate School Library (Code 2124) Monterey, California 93940 CRL-C	1
Commanding Officer & Director U.S. Navy Electronics Laboratory (Library) San Diego, California 92152 CRL-C	1
Commanding Officer Office of Naval Research Branch Off. Box 39 - Fleet Post Office New York 09510 CRL-C	5
Central Intelligence Agency Attn. CCR/DD/STD. Distribution Washington, D.C. 20505 CRL-C	1
Director, Defense Atomic Support Agency Attn. Technical Library Section Washington, D.C. 20301 CRL-C	1

DISTRIBUTION (Cont'd)

Addressee	No. of Copies
Document Receipt Notice Card Plus: Defense Documentation Center (DDC) Cameron Station Alexandria, Virginia 22314 CRL-C	20
DIA (DIAAP-142) Washington, D.C. 20301 CRL-C	1
Environmental Sciences Services Adm. Library Boulder Laboratories Boulder, Colorado 80302 CRL-C	2
FAA Bureau of Research & Development 300 Independence Avenue, S.W. Washington, D.C. 20553 CRL-C	1
Government Printing Office Library Division of Public Documents Washington, D.C. 20402 CRL-C	1
Library of Congress Aerospace Technical Division Washington, D.C. 20540 CRL-C	1
Library of Congress Exchange & Gift Division Washington, D.C. 20540 CRL-C	
NAS/NRC - Library Executive Secretary Advisory Committee to AFSC 2101 Constitution Avenue, N.W. Washington, D.C. 20418 CRL-C	1

DISTRIBUTION (Cont'd)

Addressee	No. of Copies
NASA Scientific & Technical Information Facility Attn. Acquisitions Branch (S-AK/DL) Post Office Box 33 College Park, Maryland 20740 CRL-C	1
NASA-Flight Research Center Library Post Office Box 273 Edwards, California 93523 CRL-C	1
NASA-Goddard Inst. for Space Studies (Library) 2880 Broadway New York, New York 10025 CRL-C	
NASA-Goddard Space Flight Center Technical Library Greenbelt, Maryland CRL-C	1
NASA-Jet Propulsion Laboratory Attn. Library (TDS) 4800 Oak Grove Drive Pasadena, California 91103 CRL-C	1
NASA-Langley Research Center Technical Library Langley Station Hampton, Virginia CRL-C	1
NASA-Lewis Research Center Library - Mail Stop 60-3 21000 Brookpark Road Cleveland, Ohio 44135 CRL-C	

DISTRIBUTION (Cont'd)

Addressee	No. of Copies
NASA-Manned Spacecraft Center Technical Library Houston, Texas 77058 CRL-C	1
National Center for Atmospheric Research NCAR Library, Acquisitions Boulder, Colorado 80302 CRL-C	1
ODDR&E (Library) Room 3C-128 The Pentagon Washington, D.C. 20301 CRL-C	1
Smithsonian Astrophysical Observatory - Library 60 Garden Street Cambridge, Massachusetts 02138 CRL-C	1
U.S. Atomic Energy Commission Hq. Library - Room G-017 Reports Section Washington, D.C. 20545 CRL-C	1
U.S. Weather Bureau Library - ESSA - Room 806 8060 13th Street Silver Spring, Maryland 20910 CRL-C	1
AIAA-TIS-Library 750 Third Avenue New York, New York 10017 CRL-C	1
Aerospace Corporation Attn. Library Acquisitions Group Post Office Box 95085 Los Angeles, California 90045 CRL-C	1

DISTRIBUTION (Cont'd)

Addressee	No. of Copies
Battelle Memorial Institute Library 505 King Avenue Columbus, Ohio 43201 CRL-C	1
Boeing Aero-Space Division Attn. Dr. N. L. Krisberg Post Office Box 3707 Seattle, Washington CRL-C	1
The Mitre Corporation Attn. Library Post Office Box 208 Bedford, Massachusetts 01730 CRL-C	1
The Rand Corporation Attn. Library - D 1700 Main Street Santa Monica, California 90406 CRL-C	1
TRW Systems Attn. David B. Langmuir Director, Physical Research Center One Space Park Redondo Beach, California 90278 CRL-C	1
IIT Research Institute Document Library 10 West 35th Street Chicago, Illinois 60616 CRL-C	1
The Johns Hopkins University Attn. Dr. Carl Kaplan 2500 West Rogers Avenue Baltimore, Maryland 21215 CRL-C	1

DISTRIBUTION (Cont'd)

Addressee	No. of Copies
Massachusetts Institute of Tech. Attn. Prof. Henry G. Houghton Meteorology Department 54-1712 Cambridge, Massachusetts 02139 CRL-C	1
University of California/Los Angeles Attn. Dr. Joseph Kaplan Department of Physics Los Angeles, California 90024 CRL-C	1
British Defense Staffs British Embassy Scientific Information Officer 3100 Massachusetts Avenue, N.W. Washington, D.C. 20008 CRL-C	3
Chief, Canadian Defence Research Staff 2450 Massachusetts Avenue, N.W. Washington, D.C. 20008 CRL-C	3
National Research Council National Science Library Ottawa 7, Canada CRL-C	1
Commander Naval Air Systems Command Technical Library Division (AIR-604) Department of the Navy Washington, D.C. 20360	1
Miss Sue McKinney, Librarian Physics International Company 2229 Fourth Street Berkeley, California I127	1
Materials Research Corporation Orangeburg, New York 10962 I164	1

DISTRIBUTION (Concl'd)

Addressee	No. of Copies
Massachusetts Institute of Technology Attn. Mr. Kenneth J. Button Physicist - Assistant to the Director National Magnet Laboratory, NW-14 170 Albany Street Cambridge, Mass. 02139 U62	1
Hq. AFCRL, OAR Attn. CRWA, L. C. Mansur L. G. Hanscom Field Bedford, Mass. 01730	50
Research Library - Wilmington (+ 1 reproducible)	3
Research Library - Lowell (+ 1 reproducible)	1
Reports Distribution Center - Wilmington	27

Unclassified
Security Classification

DOCUMENT CONTROL DATA - R&D
(Security classification of title, body of abstract and indexing annotation must be entered when the overall report is classified)

1. ORIGINATING ACTIVITY *(Corporate author)*
Avco Missiles, Space and Electronics Group
Space Systems Division 201 Lowell Street
Wilmington, Massachusetts 01887

2a. REPORT SECURITY CLASSIFICATION
Unclassified

2b. GROUP

3. REPORT TITLE
Synthesis of New Solid-State Materials by Ultrahigh Pressure Techniques

4. DESCRIPTIVE NOTES *(Type of report and inclusive dates)*
Final Report (14 May 1963 - 14 October 1966)

5. AUTHOR(S) *(Last name, first name, initial)*
DeLai, A. Joseph
Haag, Robert M.
Vasilos, Thomas

6. REPORT DATE	7a. TOTAL NO. OF PAGES	7b. NO. OF REFS
20 December 1966	122	33

8a. CONTRACT OR GRANT NO.	9a. ORIGINATOR'S REPORT NUMBER(S)
AF 19(628)-2943	AVSSD-0314-66-RR
b. PROJECT NO.	
c. 5621	9b. OTHER REPORT NO(S) *(Any other numbers that may be assigned this report)*
d.	AFCRL-66-737

10. AVAILABILITY/LIMITATION NOTICES
Distribution of this document is unlimited

11. SUPPLEMENTARY NOTES	12. SPONSORING MILITARY ACTIVITY
--	Electronics Research Directorate Electronics Systems Division Air Force Cambridge Research Laboratories

13. ABSTRACT

The microstructure and physical properties of dense oxides prepared at ultrahigh pressure and low temperature have been studied. Completely dense, transparent magnesium oxide has been prepared in submicron grain sizes with hardness values twice that of single crystal material and 30 percent to 50 percent greater than that of hot pressed material. A new modification of samorium oxyhydroxide has been found and characterized. X-ray determinations on the compressibility of alkali halides, RbCl, RbBr, are reported.

DD FORM 1 JAN 64 1473

Unclassified
Security Classification

Unclassified

Security Classification

14. KEY WORDS	LINK A		LINK B		LINK C	
	ROLE	WT	ROLE	WT	ROLE	WT
Solid State Materials						
High Pressure						
Compressibility						
Sound Velocity						
Magnesium Oxide						
Nickel Oxides						
Chromium Oxide						
Aluminum Oxide						
Alkali Halides						
Samarium Oxides						
Samarium Oxyhydroxide						

INSTRUCTIONS

1. ORIGINATING ACTIVITY: Enter the name and address of the contractor, subcontractor, grantee, Department of Defense activity or other organization *(corporate author)* issuing the report.

2a. REPORT SECURITY CLASSIFICATION: Enter the overall security classification of the report. Indicate whether "Restricted Data" is included. Marking is to be in accordance with appropriate security regulations.

2b. GROUP: Automatic downgrading is specified in DoD Directive 5200.10 and Armed Forces Industrial Manual. Enter the group number. Also, when applicable, show that optional markings have been used for Group 3 and Group 4 as authorized.

3. REPORT TITLE: Enter the complete report title in all capital letters. Titles in all cases should be unclassified. If a meaningful title cannot be selected without classification, show title classification in all capitals in parenthesis immediately following the title.

4. DESCRIPTIVE NOTES: If appropriate, enter the type of report, e.g., interim, progress, summary, annual, or final. Give the inclusive dates when a specific reporting period is covered.

5. AUTHOR(S): Enter the name(s) of author(s) as shown on or in the report. Enter last name, first name, middle initial. If military, show rank and branch of service. The name of the principal author is an absolute minimum requirement.

6. REPORT DATE: Enter the date of the report as day, month, year; or month, year. If more than one date appears on the report, use date of publication.

7a. TOTAL NUMBER OF PAGES: The total page count should follow normal pagination procedures, i.e., enter the number of pages containing information.

7b. NUMBER OF REFERENCES: Enter the total number of references cited in the report.

8a. CONTRACT OR GRANT NUMBER: If appropriate, enter the applicable number of the contract or grant under which the report was written.

8b, 8c, & 8d. PROJECT NUMBER: Enter the appropriate military department identification, such as project number, subproject number, system numbers, task number, etc.

9a. ORIGINATOR'S REPORT NUMBER(S): Enter the official report number by which the document will be identified and controlled by the originating activity. This number must be unique to this report.

9b. OTHER REPORT NUMBER(S): If the report has been assigned any other report numbers *(either by the originator or by the sponsor)*, also enter this number(s).

10. AVAILABILITY/LIMITATION NOTICES: Enter any limitations on further dissemination of the report, other than those imposed by security classification, using standard statements such as:

(1) "Qualified requesters may obtain copies of this report from DDC."

(2) "Foreign announcement and dissemination of this report by DDC is not authorized."

(3) "U. S. Government agencies may obtain copies of this report directly from DDC. Other qualified DDC users shall request through _____."

(4) "U. S. military agencies may obtain copies of this report directly from DDC. Other qualified users shall request through _____."

(5) "All distribution of this report is controlled. Qualified DDC users shall request through _____."

If the report has been furnished to the Office of Technical Services, Department of Commerce, for sale to the public, indicate this fact and enter the price, if known.

11. SUPPLEMENTARY NOTES: Use for additional explanatory notes.

12. SPONSORING MILITARY ACTIVITY: Enter the name of the departmental project office or laboratory sponsoring *(paying for)* the research and development. Include address.

13. ABSTRACT: Enter an abstract giving a brief and factual summary of the document indicative of the report, even though it may also appear elsewhere in the body of the technical report. If additional space is required, a continuation sheet shall be attached.

It is highly desirable that the abstract of classified reports be unclassified. Each paragraph of the abstract shall end with an indication of the military security classification of the information in the paragraph, represented as *(TS)*, *(S)*, *(C)*, or *(U)*.

There is no limitation on the length of the abstract. However, the suggested length is from 150 to 225 words.

14. KEY WORDS: Key words are technically meaningful terms or short phrases that characterize a report and may be used as index entries for cataloging the report. Key words must be selected so that no security classification is required. Identifiers, such as equipment model designation, trade name, military project code name, geographic location, may be used as key words but will be followed by an indication of technical context. The assignment of links, rules, and weights is optional.

Unclassified

Security Classification